Kinetic modelling of in vitro data of PI3K, mTOR1, PTEN enzymes and on-target inhibitors Rapamycin, BEZ235, and LY294002

Kinetic modelling of *in vitro* data of PI3K, mTOR1, PTEN enzymes and on-target inhibitors Rapamycin, BEZ235, and LY294002

Alexey Goltsov[a], Ghassan Tashkandi[b], Simon P. Langdon[b], David J. Harrison[3], James L. Bown[a,d]

[a]*School of Science, Engineering and Technology, University of Abertay, Dundee, UK;* *a.goltsov@abertay.ac.uk*
[b]*Division of Pathology, Institute of Genetics and Molecular Medicine, University of Edinburgh, Edinburgh, UK;*
s1163633@exseed.ed.ac.uk (Ghassan Tashkandib); Simon.Langdon@ed.ac.uk;
[c]*School of Medicine, University of St Andrews, St Andrews, UK;*
David.Harrison@ed.ac.uk
[d]*School of Arts, Media and Computer Games, University of Abertay, Dundee, UK;*
j.bown@abertay.ac.uk

Abstract

The phosphatidylinositide 3-kinases (PI3K) and mammalian target of rapamycin-1 (mTOR1) are two key targets for anti-cancer therapy. Predicting the response of the PI3K/AKT/mTOR1 signalling pathway to targeted therapy is made difficult because of network complexities. Systems biology models can help explore those complexities but the value of such models is dependent on accurate parameterisation. Motivated by a need to increase accuracy in kinetic parameter estimation, and therefore the predictive power of the model, we present a framework to integrate kinetic data from enzyme assays into a unified enzyme kinetic model. We present exemplar kinetic models of PI3K and mTOR1, calibrated on *in vitro* enzyme data and founded on Michaelis-Menten (MM) approximation. We describe the effects of an allosteric mTOR1 inhibitor (Rapamycin) and ATP-competitive inhibitors (BEZ2235 and LY294002) that show dual inhibition of mTOR1 and PI3K. We also model the kinetics of phosphatase and tensin homolog (PTEN), which modulates sensitivity of the PI3K/AKT/mTOR1 pathway to these drugs. Model validation with independent data sets allows investigation of enzyme function and drug dose dependencies in a wide range of experimental conditions. Modelling of the mTOR1 kinetics showed that Rapamycin has an IC_{50} independent on ATP concentration and Rapamycin is selective inhibitor of mTOR1 substrates S6K1 and 4EBP1: it retains 40% of mTOR1 activity relative to 4EBP1 phosphorylation and inhibits completely S6K1 activity. For the dual ATP-competitive inhibitors of mTOR1 and PI3K, LY294002 and BEZ235, we derived the dependence of the IC_{50} on ATP concentration that allows prediction of the IC_{50} at different ATP concentrations in enzyme and cellular assays. Comparison of the drug effectiveness in enzyme and cellular assays showed that some features of these drugs arise from signalling modulation beyond the on-target action and MM approximation and require a systems-level consideration of the whole PI3K/PTEN/AKT/mTOR1 network in order to understand mechanisms of drug sensitivity and resistance in different cancer cell lines. We suggest that using these models in systems biology investigation of the PI3K/AKT/mTOR1 signalling in cancer cells can bridge the gap between direct drug target action and the therapeutic response to these drugs and their combinations.

Keywords: kinetic modelling; PI3K; mTOR1; PTEN; Rapamycin; BEZ235

1. Introduction

The kinases, the mammalian target of Rapamycin (mTOR1/2), and phosphoinositide-3 kinase (PI3K) are central hubs in the regulation of anti-apoptotic and proliferation signalling in the PI3K/PTEN/AKT/mTOR1/S6K1 network (Cully et al., 2006; Laplante and Sabatini, 2012). Given this regulatory role, they are considered pivotal targets in cancer drug therapy (Zoncu et al., 2011). The fundamental goal in targeted therapy drug development is high therapeutic efficacy, and this efficacy is characterised not only by inhibition of the targeted protein but also by the response of the whole signalling network to on-target inhibition.

Predicting the response of the PI3K/PTEN/AKT/mTOR1/S6K1 signalling network to targeted therapy is made difficult because of pathway complexities. These complexities include multiple extra- and intra-cellular stimuli, extensive crosstalk with other signalling pathways, multiple feedforwards and feedbacks within pathways, and genetic aberrations in specific proteins (Chandarlapaty, 2012). These complexities and protein mutations within the pathway combine in ways that can induce pathway hyperactivation in cancer cells and lead to *de novo* and acquired drug resistance in different cancers (Wang et al., 2009).

The schematic in Fig. 1 shows the pathways involved in the activation of the PI3K/PTEN/AKT/mTOR1/S6K1 network by receptor tyrosine kinase (RTK) signalling. Upstream stimulation of the network results in recruitment and phosphorylation of PI3K, which then phosphorylates phosphatidylinositol 4,5 bisphosphate (PIP2) to phosphatidylinositol 3,4,4-triphosphate (PIP3). The second lipid messenger PIP3 in turn recruits downstream proteins to the plasma membrane and this leads to phosphorylation of AKT and PDK1 kinases. Phosphatase and tensin homolog deleted on chromosome ten (PTEN) dephosphorylates PIP3 into PIP2. A normal function of PI3 kinase and phosphatase PTEN strictly control the response of AKT signalling to RTK stimuli (Goltsov et al., 2012). The most common aberrations in the PI3K/PTEN cycle, observed in 80% of cancers, are loss of PTEN and/or PIK3CA mutations that cause activation of the PI3K/PTEN/AKT/mTOR1/S6K1 signalling network independently of RTK signals, which can lead to tumourigenesis and drug resistance (Nik-Zainal et al., 2016; Stemke-Hale et al., 2008).

mTOR acts as a key downstream integrator of PI3K/PTEN/AKT signalling and the serine/threonine protein kinase assembles into two complexes, mTOR1 and mTOR2: mTOR1 is a major regulator of cap-dependent translation and elongation via phosphorylation of 4EBP1 and S6K1 respectively (Siddiqui and Sonenberg, 2015); mTOR2 phosphorylates AKT(Ser437) (Cully et al., 2006). Besides kinase catalytic domains, mTOR has several domains (FAT, HEAT, FAT, FRB) acting as structural scaffolding for different subunits of the mTOR1 and mTOR2 complexes (Raptor, Rictor, PRAS40, and mSLT8) which regulate its binding to substrate/activator, catalytic activity and localisation (Yang et al., 2013). Phosphorylation of S6K1 at multiple phospho-sites by both mTOR1 and PDK1 (Phosphoinositide-dependent kinase-1) forms feedforward and feedback loops in the PI3K/PTEN/AKT/mTOR1/S6K1 pathway (Fig. 1). These feedback loops, together with crosstalk with the MAPK pathway and mTOR1 autoregulation through protein-protein interactions, mean that drug action must account for system-scale properties. That is, the response of the output signal is defined by properties of the whole signalling network, since it is the whole network that modulates functioning of the specific drug targeted proteins.

Multiple drugs targeting this pathway are in clinical practice or preclinical development (Kalachand et al., 2011; Markman et al., 2010), and here we focus on Rapamycin and BEZ235 (Mita et al., 2016). We also consider LY294002 because of its common use in studies of the

response of PI3K/AKT pathway to inhibition in different cancer cell lines (Vlahos et al., 1994; Walker et al., 2000). Rapamycin is a mTOR-targeting molecule isolated from bacteria and used as an antifungal and immunosuppressive drug (Laplante and Sabatini, 2012; Wang et al., 2009). In preclinical studies, Rapamycin has shown anti-tumour effects against various tumour types including breast cancer, glioblastoma, rhabdomyosarcoma by controlling cell survival, angiogenesis and proliferation (Laplante and Sabatini, 2012; Wang et al., 2009). Temsirolimus, a rapamycin rapalog, was approved to treat progressive renal cell carcinoma in the clinic (Hudes et al., 2007). Although Rapamycin rapalogs have shown promising antitumour effects in preclinical studies, most of the clinical trial outcomes were disappointing. The existence of several feedback loops in the PI3K/AKT/mTOR pathway may have played an important role in the limitation of Rapamycin in addition to its inadequacy in blocking mTORC2 (Harrington et al., 2004; Jacinto et al., 2004; Yu et al., 2011).

Both PI3K and mTOR belong to the PI3K-related kinase (PIKK) family, and so both might be inhibited by the same ATP competitive inhibitors, resulting in dual activity against both targets. BEZ235 is a potent PI3K/mTOR dual inhibitor that blocks both class I PI3K and mTOR1/2 through competition for the ATP-binding sites of these enzymes (Maira et al., 2008). *In vitro* and *in vivo* studies have shown its high anti-proliferative activities in neoplastic cells as well as a reduction in the phosphorylation level of AKT and its downstream proteins (Jebahi et al., 2014; Maira et al., 2008; Serra et al., 2008). BEZ235 is currently in phase 1/2 clinical trials and is being tested against a number of solid tumours including breast, endometrial, renal and pancreatic tumours. Results show good dose toleration but limited clinical response as a monotherapy or in combination with other drugs (Bendell et al., 2015).

LY294002 is an ATP competitive inhibitor of PI3K (p110α/β) and, although it is not in clinical practice due its toxicity, it is widely used in numerous cell line studies to inhibit the PI3K/AKT pathway. Studies have revealed that LY294002 is not specifically selective for PI3K and can have off-target effects, and mTOR is among those off-targets impacted by LY294002 (DNA-dependent kinase (DNA-PK), casein kinase (2CK2), GSK3β) (Gharbi et al., 2007; Toral-Barza et al., 2005). Accordingly, some of these off-target effects of LY294002 relate to the PI3K/AKT/mTOR pathway and might contribute to the overall inhibition effect observed upon cell treatment. Toral-Barza et al. (Toral-Barza et al., 2005) showed that LY294002 is a PI3K/mTOR dual inhibitor that blocks PI3K and mTOR kinase through an ATP-competitive mechanism.

Studies on the PI3K/PTEN/AKT/mTOR1/S6K1 pathway reveal clear discrepancies among drug efficacy readouts at the target, pathway and cellular levels for different cancer cell lines (Hassan et al., 2014; Santiskulvong et al., 2011; Shoji et al., 2012). These observed discrepancies are likely due to a mix of the complexity of the signalling network and its mutations together with fundamental differences in enzyme kinetics in various cellular environments. In particular, intracellular conditions in cancer cells may be significantly different to experimental conditions in enzymatic assays, e.g. substrate and cofactor concentrations (Acker and Auld, 2014). To inform the comparison of drug efficacies obtained in enzymatic and cellular assays, and to combine the data derived from these assays, we need data on protein and inhibition kinetics in different cancer cells in different conditions. In general, key intracellular conditions cannot be modelled in enzymatic assays but these can be modelled in *in silico* experiments using enzyme kinetic models that describe enzyme and inhibitor properties in a wide region of environmental conditions.

This paper provides a systems biology framework to integrate kinetic data from enzymatic and cellular assays into a unified kinetic model. Fig. 2 shows a schematic of this framework, where data describing enzyme activity following drug action may be combined with

enzyme kinetic data to predict the IC_{50} for drugs in different cellular conditions. Integration of various kinds of experimental data is motivated by a need to increase accuracy in kinetic parameter estimation and therefore the predictive power of the systems biology models. Accurate estimations of enzyme kinetic parameters are needed to 'bridge the gaps in systems biology' (Cvijovic et al., 2014) by reducing model uncertainty. A well calibrated model can be used to help explain the observed discrepancies of enzyme function and drug effects in different experimental conditions, in different cellular environment as well as in analysis of enzyme mutation effects of drug action in various cellular lines.

Previous models of enzyme kinetics that are based on detailed kinetic mechanisms and integration of a wide range of *in vitro* experimental data can be found e.g. for Rho GTPases (Goryachev and Pokhilko, 2006), the adenine nucleotide translocase (Metelkin et al., 2009), and S6K1 protein kinase (Keshwani and Harris, 2008). We extend these approaches by demonstrating the incorporation of experimental data that characterises enzymatic response to drug action to inform model construction. Here, as an exemplar use of this framework we present kinetic models of purified enzymes PI3K, mTOR1 and PTEN that describe their catalysis mechanisms. We apply these models to investigate the effects of allosteric (Rapamycin) and ATP-competitive (BEZ235, L294002) inhibitors of mTOR1 and PI3K. We use Michaelis-Menten (MM) approximation in our model formulation combined with *in vitro* protein assay data on enzyme kinetics to calibrate and then validate the models. In line with the increasing publications devoted to the expansion of MM approximation and its application in metabolic and signalling network investigation (Cornish-Bowden, 2013; Schnell, 2014; Tummler et al., 2014) we test whether the kinetics of these kinases and phosphatase can be described in MM approximation and reproduce such indicators as kinetic curves, inhibition constants, dose dependencies and IC_{50} values. We compare drug activities in purified protein assays and those in cancer cell populations in order to determine those drug properties which can be described by MM kinetics and those properties that lie beyond this approximation and depend on an understanding of the whole signalling network response. We also discuss an application of this comparative analysis to translation of *in vitro* data on drug activity to therapeutic drug efficacy.

2. Methods

The schematic of our approach is shown in Fig. 2. For model development, calibration and validation we used two types of experimental data: dependencies of enzyme activity on substrate concentrations measured in the absence and presence of drugs and dose dependencies of enzyme inhibition on drug concentrations. The developed approach allows us to integrate kinetic experimental data obtained under different experimental conditions. Integrating data increases model reliability and accuracy with respect to kinetic parameter estimation because of an increase in the set of experimental points used in that estimation over separate experimental data sets (Cornish-Bowden, 2014). Moreover, we also make use of molecular structural data on enzyme-substrate and enzyme-drug complexes to support model formulation. Specifically, involvement of these structural data can serve to discriminate among different candidate mechanisms of drug action, e.g. inhibition of enzyme activity or substrate affinity. We can validate the model on independent data sets and then this validated model may be used to investigate enzyme functions in experimental conditions beyond those used in its construction.

Fitting of experimental data was carried out using the constrained nonlinear optimization method running Matlab (MathWorks Inc.). Standard errors and confident intervals of the kinetic

parameters obtained in fitting were estimated using the bootstrap method (Draper and Smith, 2014; Efron and Tibshirani, 1994). In the bootstrap procedure we used a resampling process for the *n* residues

$$\boldsymbol{e} = \boldsymbol{Y}_{exp} - \boldsymbol{Y}_{mod}\ ,$$

where $\boldsymbol{Y}_{exp}$ and $\boldsymbol{Y}_{mod}$ are vectors of the experimental data and the best fitted model results; $\boldsymbol{e}$ is a vector of the residues of dimension *N* corresponding to a number of experimental points. Then we generate *M* bootstrap residues vector $\boldsymbol{e}_i^*$ where each element is chosen from the elements of the residue vector $\boldsymbol{e}$ with probability 1/*n*. At the next step of the bootstrap procedure, the model is fitted against bootstrap samples

$$\boldsymbol{Y}_{exp,i}^* = \boldsymbol{Y}_{exp} + \boldsymbol{e}_i^*$$

to define the estimates of *M* samples of kinetics parameters $\boldsymbol{k}_i$.

As an estimate of kinetic parameter k_l we use the median of *M* bootstrap samples for parameter k_l obtained in the fitting procedure. As a bootstrap confidence interval (CI) we calculate the percentile confidence interval $(k_{l,low}\ ;\ k_{l,up})$, where $k_{l,low}$ and $k_{l,up}$ are 2.5th and 97.5 percentile of the distribution of k_l obtained in the bootstrap process (Efron and Tibshirani, 1994). We compared these estimate of parameters k_l with the mean values $\overline{k_l}$ of M bootstrap samples and the standard normal confidence interval $(\overline{k_l} - 1.96 \cdot SE_l;\ \overline{k_l} + 1.96 \cdot SE_l)$ for the 95% CI where SE_l is the estimate of standard error of bootstrap mean of kinetic parameter $\overline{k_j}$

$$SE_l = \left(\sum_{i=1}^{M} \left(k_{il} - \overline{k_l}\right)^2 / (M-1) \right)^{1/2} .$$

2.1 Kinetic model of mTOR1 complex and its inhibition

We developed a kinetic model of the catalytic cycle of the mTOR1 complex that catalyses phosphorylation of S6K1 and 4EBP1 kinases (Fig. 3). The model was developed in accordance with the framework of a two substrate random bi-bi mechanism of enzymatic reaction using an approximation of fast binding of substrates (ATP, S6K1 and 4EBP1) (Cornish-Bowden, 2004). In the catalytic cycle we considered the allosteric inhibitor of mTOR1, Rapamycin (Rap), and two ATP-competitive inhibitors, BEZ235 and LY294002. According to experimental data, Rapamycin binds with low affinity (26 μM (Banaszynski et al., 2005)) to the FRB domain of mTOR (FKBP-rapamycin binding domain) and its binding becomes much stronger in the presence of FKBP12 protein (FK506-binding protein 12). The high affinity of Rapamycin with FKBP12 protein (0.2 nM (Banaszynski et al., 2005)) leads to Rapamycin binding to mTOR1 through the formation of the trimeric complex FKBP12-Rapamycin-FRB with dissociation constant 12±0.8 nM (Banaszynski et al., 2005). In the catalytic cycle we included the mTOR1 binding reaction in the absence and presence of the FKBP12 with dissociation constant $K_{d,Rap1}$ and $K_{d,Rap2}$ respectively. Considering these data, and other experimental data on inhibition of S6K1 and 4EBP1 phosphorylation by mTOR1 (Choo et al., 2008; Tao et al., 2010; Toral-Barza et al., 2005), we assumed that mTOR1 binding to Rapamycin or Rapamycin-FKBP complexes retains its residual catalytic activity relating to 4EBP1 and causes its full suppression relating to S6K1 (see Fig. 3).

In line with the developed catalytic cycle (Fig. 3) we derived rate equations of the phosphorylation of 4EBP1, V_{4EBP1}, and S6K1, V_{S6K1}, according to a random bi-bi mechanism approximation for a two substrate reaction (Cornish-Bowden, 2004; Demin and Goryanin, 2008) as follows:

$$V_{4EBP1} = \frac{k_{4EBP1} \cdot mTOR1 \cdot 4EBP1 \cdot ATP}{K_{d,4EBP1} \cdot K_{d,ATP} \cdot \Delta_{mTOR}} (1 + \eta_{4EBP1} \cdot R) \quad (1)$$

$$V_{S6K1} = \frac{k_{S6K1} \cdot mTOR1 \cdot S6K1 \cdot ATP}{K_{d,S6K1} \cdot K_{d,ATP} \cdot \Delta_{mTOR}}, \quad (2)$$

where

$$\Delta_{mTOR} = \left(1 + \frac{ATP}{K_{d,ATP}} + \frac{LY}{K_{d,LY}} + \frac{BEZ}{K_{d,BEZ}}\right)\left(1 + \frac{4EBP1}{K_{d,4EBP1}} + \frac{S6K1}{K_{d,S6K1}}\right)(1 + R),$$

$$R = \frac{Rap}{K_{d,Rap1}} + \frac{Rap\_FKBP}{K_{d,Rap2}}.$$

Here $K_{d,i}$ are the dissociation constants of substrates 4EBP1 and S6K1 and inhibitors Rapamycin (Rap), BEZ235 (BEZ), and LY294002 (LY); k_{4EBP1} and k_{S6K1} are catalytic rates. $\eta_{4EBP1} = k_{4EBP1,Rap}/k_{4EBP1}$ is the inhibition coefficient of mTOR reaction rate for 4EBP1 phosphorylation by Rapamycin which is equal to the ratio of residual catalytic activity of mTOR1-Rapamycin complex, $k_{4EBP1,Rap}$, to the catalytic activity of mTOR1, k_{4EBP1}. Equations (1) and (2) thus describe the competitive kinetics of the two substrates 4EBP1 and S6K1 for enzyme mTOR1, and this corresponds to the two-substrate reactions catalysed by mTOR1 in cells.

2.2 Kinetic model of PI3K and its inhibition by LY294002 and BEZ235

A model of the catalytic cycle of PI3K catalysing the phosphorylation of PIP2 was developed using the same MM approximation as in the case of mTOR1 modelling (Fig. 4). In the catalytic cycle we considered the same ATP competitive inhibitors, LY294002 and BEZ235.

In line with the PI3K catalytic cycle (Fig. 4), we derived rate equations of PIP2 phosphorylation, V_{4EBP1}, according to a two-substrate reaction proceeding through a random bi-bi mechanism (Cornish-Bowden, 2004; Demin and Goryanin, 2008):

$$V_{PI3K} = \frac{k_{PI3K} \cdot PI3K \cdot PIP2 \cdot ATP}{K_{d,PIP2} \cdot K_{d,ATP} \cdot \Delta_{PI3K}} \quad (3)$$

where

$$\Delta_{PI3K} = \left(1 + \frac{PIP2}{K_{d,PIP2}}\right)\left(1 + \frac{ATP}{K_{d,ATP}} + \frac{LY}{K_{d,LY}} + \frac{BEZ}{K_{d,BEZ}}\right)$$

2.3 Kinetic model of PTEN

To model PTEN kinetics we used experimental data on PTEN activity, measured in unilamellar mixed phosphatidylcholine vesicles containing lipid substrate PIP3 (McConnachie et al., 2003). In this experiment bulk concentration of substrate PIP3 was varied at different fixed surface concentrations of PIP3, X_{PIP3} (mole fraction), in the vesicles. As a result, the dependence of PTEN activity with respect to hydrolysing of PIP3 on bulk concentration of PIP3 at the different X_{PIP3} was obtained. To model these kinetic data, we used a MM rate equation:

$$V_{PTEN} = \frac{k_{PTEN} \cdot PTEN \cdot PIP3}{K_{PIP3} + PIP3_s} \quad (4)$$

where k_{PTEN} and K_{PIP3} are catalytic and Michaelis constants respectively and $PIP3_s = X_{PIP3}PIP3$.

3. Results

3.1. mTOR1 kinetic model parameterisation and validation through drug action

To determine the kinetic parameters of Eqs. (1) and (2) we used *in vitro* experimental data on the phosphorylation of 4EBP1(Thr46) and S6K1(Thr389) by mTOR kinase (Tao et al., 2010; Toral-Barza et al., 2005). Reproducing the experimental conditions of these *in vitro* experiments in our *in silico* model, we carried out the joint fitting of a set of experimental data including the dependencies of reaction rate V_{4EBP1} (Eq. (1)) on 4EBP1 concentration and also on ATP concentration at different concentrations of Rapamycin (Tao et al., 2010). Experimental data and the results of fitting are shown in Fig. 5A and 5B. A set of obtained kinetic parameters along with the results of the bootstrap procedure (see Method) are given in Table 1. As a result of the bootstrap procedure, we obtained bootstrap samples of kinetic parameters and gave the medians and the 95% percentile confidence interval for each parameters. The number of bootstrap samples in our calculations was 200 to ensure stable values of the medians and CVs. We also calculated the means and the standard normal confidence interval (see Methods) for the bootstrap samples and gave them in Table S1 in Supplement 6. Comparison of the means, medians, and CIs of the kinetics parameters obtained by two methods revealed similar results.

According to modelling, mTOR kinase retains a fraction of its activity following Rapamycin inhibition due to its residual catalytic activity. Results of the fitting showed that mTOR1 retains 40% of catalytic activity at Rapamycin binding: the catalytic rate k_{4EBP1} is changed by the factor η_{4EBP1} =0.42 μM CI(10^{-3}; 0.5) in the presence of Rapamycin (see the residual level of kinase activity in Fig. 5C and Table 1). The dissociation constant $K_{d,Rap2}$=6 nM CI(3.1; 6.9); obtained through fitting is close to the experimental value 12±4.2 nM and for the trimeric complex FKBP12-Rapamycin-FRB measured by surface plasmon resonance (SPR) methods (Banaszynski et al., 2005). The value of the dissociation constant of ATP, $K_{d,ATP}$ =8.4 μM CI(6.2; 8.9) obtained in our calculation, is substantially smaller than the value of the Michaelis constant 74 μM obtained in (Tao et al., 2010) based on the fitting of experimental data by the Michaelis-Menten equation (Fig. 5B). This discrepancy may be due to the facts that first we used a wider range of experimental data in the fitting procedure than used in (Tao et al., 2010) and second we defined the dissociation constant of ATP, $K_{d,ATP}$, in our model rather than the apparent Michaelis constant obtained in (Tao et al., 2010).

To validate the model with the obtained set of kinetic parameters we calculated the concentration dependence of mTOR1 activity (Eq. (1)) on Rapamycin concentration and found satisfactory agreement with the experimental dose dependence (Fig. 5C, line 1). We also calculated the dose dependence of mTOR1 activity on the concentration of BEZ235 (Fig. 5C, line 2). Comparison of the two dose dependencies for Rapamycin and BEZ235 shows that Rapamycin inhibits 60% of mTOR1 catalytic activity while BEZ235 suppresses activity totally (Fig. 5C). In this calculation, we determined the dissociation constant of BEZ235, $K_{d,BEZ}$, via the fitting of this single parameter of the model (Eq. (1)) against the experimental dose dependence on reaction rate inhibition of truncated mTOR kinase (Tao et al., 2010). The obtained dissociation constant, $K_{d,BEZ}$=0.56 nM CI(0.48; 0.57), is close to the Michaelis constants K_m=2.5 nM and 1.7 nM obtained based on the Michaelis-Menten equation fitting to radiometric and FRET assay data respectively (Tao et al., 2010) (Table 1). The obtained dissociation constant $K_{d,BEZ}$ allows calculation of the

IC_{50} value at the ATP concentration used in the experimental assay according to the following equation

$$IC_{50} = K_{d,BEZ}\left(1 + \frac{ATP}{K_{d,ATP}}\right). \quad (5)$$

Eq. (5) follows from Eq. (1) and a definition of the IC_{50} value as the inhibitor concentration corresponding to a 50% inhibition of reaction rate V_{4EBP1} (derivation of Eq. (5) is given in Supplement 1). At concentration ATP=100 μM Eq. (5) gives IC_{50} = 8 μM that is close to the experimental value of IC_{50} = 10 nM obtained from the experimental dose dependence (Tao et al., 2010) (see experimental data in Fig. 5C). Accordingly, Eq. (5) parameterised with an ATP-competitive mTOR1 inhibitor allows calculation of the IC_{50} values for BEZ235 at different ATP concentrations in an experimental assay and estimation of BEZ235 IC_{50} for different cells using a known ATP concentration.

In contrast to IC_{50} dependence (Eq. (5)) for the ATP-competitive inhibitor, the IC_{50} for the allosteric inhibitor Rapamycin does not depend on ATP concentration and according to Eq. (1) is equal to its dissociation constant:

$$IC_{50} = K_{d,Rap}\,, \quad (6)$$

where $K_{d,Rap}$ is either dissociation constant $K_{d,Rap1}$ or $K_{d,Rap2}$ depending the absence or presence of the FKBP12 protein in assays. This exact equality follows from the equation of reaction rate V_{4EBP1} Eq (1) (see derivation in Supplement 2). Comparison of the experimental IC_{50}=9.6 nM (+FKBP12) and IC_{50}>1 μM (no FKBP12) with the theoretical values $K_{d,Rap2}$ =6 nM CI(3.1; 6.9) and $K_{d,Rap1}$ =1.7 μM CI(1.3; 1.8) confirms this relationship.

To determine the kinetic parameters of mTOR1 related to the phosphorylation reaction of S6K1 kinase as described by Eq. (2) we used *in vitro* experimental data on the dependence of the reaction rate of S6K1(T389) phosphorylation on ATP concentration at different concentrations of LY294002 inhibitor (Toral-Barza et al., 2005). Given that LY294002 is a nonspecific inhibitor of PI3K (Vlahos et al., 1994), and considering the high homology in catalytic sites between PI3K and TOR kinases (Yang et al., 2013), we assumed that LY294002 inhibits mTOR1 by a similar mechanism to PI3K (see mTOR1 catalytic cycle in Fig. 3). Results of the fitting are shown in Fig. 6A and kinetic parameters obtained are given in Table 1. To demonstrate clearly that LY294002 is an ATP-competitive inhibitor of mTOR kinase, we also presented theoretical and experimental kinetic data in the Lineweaver-Burk plot in Supplement 3.

To obtain the dissociation constants of Rapamycin binding to mTOR1, $K_{d,Rap1}$ and $K_{d,Rap2}$, we used the experimental dose dependence of the inhibition of S6K1(Thr389) phosphorylation reaction rate by Rapamycin (Toral-Barza et al., 2005). Given the derived kinetic parameters (Table 1) and concentrations of species in the experimental assay (Toral-Barza et al., 2005) we defined $K_{d,Rap1}$=1.7 μM CI(1.3; 1.8); and $K_{d,Rap2}$=1.6 nM CI(1.2; 1.7) in the absence and presence of FKBP12 respectively (Fig. 6B). The obtained values in the presence of FKBP12 are in agreement with nanomole values of dissociation constant: 0.35 nM and 12±0.8 nM obtained by fluorescence polarization assay (FPA) and SPR methods respectively (Banaszynski et al., 2005). The experimental dissociation constant in the absence of FKBP12 is 490±39 nM and 26±0.8 μM obtained by FPA and SPR methods respectively (Banaszynski et al., 2005). Note that the values of dissociation constants of Rapamycin and mTOR kinase domain obtained in the model and those from experimental methods are close to the experimental values of IC_{50}=2 nM in the presence of FKBP12 and IC_{50}> 1 μM in the absence of FKBP12 in the experimental assay of

S6K1(Thr389) phosphorylation (Toral-Barza et al., 2005), and these values conform to the relationship between K_d and IC_{50} values given by Eq. (6) for an allosteric inhibitor.

To validate the mTOR1 model (Eq. (2)) with the parameter set (Table 1) we calculated the dose dependence of inhibition of S6K1(Thr389) phosphorylation by LY294002 (Fig. 6C), and compared the results with experimental data (Toral-Barza et al., 2005). In a similar manner to Eq. (5) the dependence of IC_{50} for LY294002 on ATP concentration is given by the equation

$$IC_{50} = K_{d,LY}\left(1 + \frac{ATP}{K_{d,ATP}}\right), \quad (7)$$

which allows us to obtain the LY294002 IC_{50} value at the ATP concentration used in the experimental assay. At ATP concentration of 100 μM (Toral-Barza et al., 2005), Eq. (5) gives IC_{50}=1.5 μM that corresponds to the experimental IC_{50} value obtained in this experiment (see experimental data in Fig. 6C). Accordingly, the satisfactory parameterisation of Eq. (7) for LY294002 may be used to calculate the LY294002 IC_{50} values at different concentrations of ATP in *in vitro* assays.

We applied Eq. (7) to calculate the dose dependence of mTOR1 for LY294002 at 2 μM ATP and compared the obtained result with that calculated at 100 μM ATP (lines 1 and 2 in Fig. 6C). As LY294002 is an ATP-competitive inhibitor of mTOR1, the IC_{50} decreases when ATP decreases (IC_{50}=0.15 μM at 2 μM ATP). Modelling showed that LY294002 becomes a stronger inhibitor of mTOR1 at low ATP concentrations in the range 1 μM - 10 μM, which corresponds to ATP concentration in mammalian cells (McLaughlin et al., 2002). Note, according to Eq. (6), the inhibition activity of the allosteric inhibitor Rapamycin does not depend on ATP concentration. To investigate synergistic effects of the combination of the allosteric inhibitor Rapamycin with the ATP-competitive inhibitor LY294002 we calculated the dose dependence of mTOR1 inhibition on LY294002 concentration at 10 nM Rapamycin and 100 μM ATP (line 3 in Fig. 6C). The calculation revealed an additive effect of the two inhibitors and an increase of the LY294002 IC_{50} value from 1.5 μM to 30 μM when in combination with Rapamycin. Thus results do not indicate any synergistic effects of Rapamycin and LY294002 in combination.

3.2 *PI3K kinetic model parameterisation and validation through drug action*

The kinetic parameters of PI3K were derived by fitting of reaction rate V_{PI3K} (Eq. (3)) against *in vitro* experimental data on the phosphorylation of PIP2 (Huang et al., 2011; Vlahos et al., 1994). Figs. 7A, B, and C show the results of fitting of the dependencies of the reaction rates on ATP and PIP2 concentrations in the absence and presence of LY294002 inhibitor. The form of the fitted Lineweaver-Burk plot confirms that LY294002 is an ATP-competitive inhibitor of PI3K (Fig. 7C). The obtained kinetic parameters of the kinase and dissociation constant of LY294002 are provided in Table 2.

To estimate the dissociation constant of BEZ235 we applied the PI3K model to describe the dose dependence of ADP release on the inhibitor concentration for PI3Kα enzyme (Maira et al., 2008). To reproduce experimental data (Maira et al., 2008), we modelled ADP production by an ordinary differential equation with the initial conditions corresponding to the experimental assay:

$$\frac{dADP}{dt} = V_{PI3K}\,, \quad (8)$$

where reaction rate V_{PI3K} is defined by Eq. (3). The dissociation constant obtained as a result of best fitting of experimental dose dependence of ADP production on BEZ235 concentration (see Fig. 7D, line 1) is provided in Table 2 with experimental data on K_i and IC_{50} values for BEZ235 available from literature. We also used similar experimental data (Maira et al., 2008) to calculate the dose dependence for the LY294002 inhibitor. Comparison of the dose dependencies for BEZ235 and LY294002 is shown in Fig. 7D by lines 1 and 2 respectively. The dissociation constant $K_{d,LY}$=0.1±0.02 μM obtained for PI3Kα isoform as a result of the best fitting of experimental dose dependence is less than $K_{d,LY}$=0.7±0.1 μM obtained above for bovine brain PI3K isolated in experimental work (Vlahos et al., 1994). The obtained dissociation constant $K_{d,LY}$=0.1±0.02 μM is close to the dissociation constant $K_{d,LY}$=0.21±0.04 μM for the PI3Kγ isoform measured by the intrinsic tryptophan fluorescence method (Walker et al., 2000).

To validate the calibrated model of PI3K (Eqs. (3) and (8)) we used the model to describe the experimental dependence of the IC_{50} value for BEZ235 and LY294002 on ATP concentration measured for dose dependence of ADP production for a PI3Kγ enzyme assay (Maira et al., 2008). The theoretical ATP dependence of the IC_{50} values for BEZ235 and LY294002 was obtained based on the analytical solution of Eq. (8). As a solution of Eq. (8) cannot be written explicitly we expressed the dependence of the IC_{50} value on the initial ATP concentration ATP_0 in the form

$$IC_{50} = K_{d,i}\left(\frac{ln\left(\frac{ATP_{I0}}{ATP_0}\right) - Bt_m}{2ln\left(\frac{1}{2}\left(1+\frac{ATP_{I0}}{ATP_0}\right)\right)} - 1\right), \qquad (9)$$

where

$$B = \frac{k_{PI3K}\cdot PI3K\cdot PIP2}{K_{d,PIP2}\cdot K_{d,ATP}}\left(1+\frac{PIP2}{K_{d,PIP2}}\right)^{-1}.$$

Here $ATP_{I0} = ATP(t_m, I=0)$ is the final concentration of ATP at the reaction terminal time t_m in the absence of inhibitors which can be defined from Eq. (8). The detailed derivation of Eq. (9) is given in Supplement 4. The obtained Eq. (9) allows calculating dependence of the IC_{50} value on the initial concentration ATP_0 based on the solution of Eq. (8) $ATP(t_m, I=0) = ATP_0 - ADP(t_m, I=0)$ in the absence of inhibitors. Note using of this equation to does not require calculation of dose dependence for the inhibitor at the different concentrations of ATP and numerical estimation of IC_{50} values. The dependencies of the IC_{50} value for BEZ235 and LY294002 on ATP_0 concentration was calculated based on Eq. (9) with kinetic parameters obtained in the fitting procedure (Table 2) and the initial concentrations of the substrates corresponding to the experimental conditions in the work (Maira et al., 2008). Dissociation constants for BEZ235 and LY294002 in these calculations were $K_{d,BEZ} = 2$ nM and $K_{d,LY} = 0.7$ μM which lie within the obtained CI of these parameters (Table 2).

In Fig. 8A, we compared the obtained theoretical dependencies with experimental data (Maira et al., 2008). The linear dependence of the IC_{50} values on ATP_0 concentration obtained in the model corresponds to the ATP-competitive mechanism for BEZ235 and LY294002 inhibitors (Fig. 8A and 8B respectively) and satisfactorily describes the observed experimental dependencies of the IC_{50} values for these inhibitors (Maira et al., 2008). To investigate the value where the line intercepts the IC_{50}-axis, we plot the linear dependence of the IC_{50} values on ATP concentration (dotted lines in Figs. 8A and 8B) obtained based on the dose dependence of the reaction rate V_{PI3K} on the inhibitor concentration (Eqs. (5) and (7)). Exact coincidence between two lines shows equivalence of the IC_{50}measurement in both *in vitro* assays at the specific

experimental conditions. Therefore, the intercept of the regression line may serve as an estimate of dissociation coefficients of ATP-competetive inhibitors. For the LY294002 and BEZ235 IC_{50}s, we got estimates for $K_{d,BEZ} = 2$ nM and $K_{d,LY} = 0.7$ μM respectively that satisfactorily agrees with the fitted values of these dissociation constants (Table 2). Thus experimental data IC_{50} on ATP concentration for ATP-competitive inhibitors can be used to estimate dissociation constant of the inhibitors.

3.3 PTEN kinetic model parameterisation

Fig. 9 (lines) shows the fitting of the reaction rate V_{PTEN} (Eq. (4)) depending on PIP3 concentration at four surface concentrations of PIP3, X_{PIP3} (mole fraction), against experimental data (McConnachie et al., 2003). As a result of fitting, a low value of the Michaelis constant was obtained, K_{PIP3}=29 nM (20; 31) nM. Plotting theoretical and experimental data in the reciprocal axes, $1/PIP3$ and $1/V_{PTEN}$, showed that the rate equation in the form (Eq. (8)) describes satisfactorily the kinetic behaviour of V_{PTEN} at different X_{PIP3}. Moreover the straight lines corresponding to different X_{PIP3} intersect the $1/V_{PTEN}$ axis at the same point, which means that maximum rate of PTEN is independent of X_{PIP3}, and the reaction rate V_{PTEN} depends on the concentration of PIP3 in the membrane ($X_{PIP3} \cdot PIP3$) according to Eq. (4).

Discussion

The results of our kinetic modelling of PI3K, mTOR1 kinases and PTEN phosphatase showed that *in vitro* kinetics of these purified proteins can be described satisfactorily with Michaelis-Menten approximation, i.e. with a fast substrate binding approximation. The obtained kinetic parameters of these proteins are partly in agreement with those obtained previously by the fitting of MM equations against separate kinetic curves (Maira et al., 2008; Tao et al., 2010; Toral-Barza et al., 2005). In line with the schematic in Fig. 2 we enhanced the estimation of a number of kinetic parameters of PI3K and mTOR1 kinases through the application of two-substrate reaction rate equations calibrated against experimental data describing kinetics in different experimental conditions. This calibration approach allowed us to estimate dissociation constants of the substrates instead of apparent Michaelis constants that depend on experimental assay conditions such as the second substrate concentration in two-substrate reactions. The developed models were then applied to describe allosteric inhibition of mTOR kinase by Rapamycin and ATP-competitive inhibition of PI3K and mTOR kinases by LY294002 and BEZ235.

Modelling of the mTOR kinase showed high selectivity of allosteric inhibitor Rapamycin to mTOR1 substrates: Rapamycin differentially regulates mTOR1 activity relating to its substrates S6K1 and 4EBP1. In the model, Rapamycin changes the catalytic rate of 4EBP1 phosphorylation k_{4EBP1} by a factor of η_{4EBP1}=0.4 (Fig. 5C and Table 1). Analysis of the kinetic data and dose dependence showed that mTOR1 retains 40% of catalytic activity without a change in dissociation constant to the substrate, $K_{d,4EBP1}$ (Fig. 5). In contrast, Rapamycin both alone and in a complex with FKBP12 inhibits completely the catalytic activity of mTOR1 relating to S6K1 phosphorylation (η_{S6K1}=0). In agreement with experimental data, the modelling showed that Rapamycin completely inhibits S6K1 phosphorylation at a Rapamycin concentration greater than 0.1 μM and 100 μM in the presence and absence of FKBP12 respectively (Shor et al., 2008) (Fig. 6D).

Experimental investigations into the crystal structure of a truncated mTOR kinase (Yang et al., 2013) suggest that the binding of Rapamycin-FKBP12 complex near the mTOR substrate-binding site inhibits kinase activity due to restricting the accessibility of the substrates to the recessed catalytic cleft. As per the schematic in Fig. 2, we can integrate this knowledge into the model. According to our modelling, the Rapamycin-FKBP12 complex does not compete with mTOR1 substrates and it binds to mTOR1 jointly with either 4EBP1 or S6K1 kinases and forms triple complexes in the form Rapamycin-FKBP1-mTOR-Substrate as depicted in the scheme of the mTOR catalytic cycle (Fig. 3). In the model, Rapamycin decreases the mTOR1 catalytic rate relating to 4EBP1 and S6K1 without impacting mTOR1 affinity to substrates (Table 1). This decrease in catalytic rate may result from the observation that the Rapamycin-FKBP12 complex perturbs the positioning of the substrate at the catalytic site but does not influence significantly substrate binding. We suggest that the observed differences in catalytic rate is responsible for Rapamycin selectivity to mTOR1 substrates and this property might be due to steric effect stemming from the different sizes of S6K1 and 4EBP1 proteins: 60 KDa and 18 KDa respectively. Thus the active site restriction mechanism proposed in (Yang et al., 2013) corresponds to the negative regulation mechanism of catalytic rate in our model.

Yang et al. (Yang et al., 2013) propose a biparticle substrate-recruitment mechanism for S6K1 binding to the mTOR active site, according to which the FRB provides a secondary binding site for the substrate near the entrance to the catalytic cleft. They suggest that this Rapamycin-binding site participates in substrate binding with the recessed active site of mTOR. In our kinetic modelling, Rapamycin both alone and in a complex with FKBP12 does not change the dissociation constants of either substrate 4EBP1 or S6K1, and only influences the catalytic rate of the enzyme. Accordingly, we suggest that either: 1) our analysis of kinetic data is not sensitive to the biparticle substrate-recruitment mechanism suggested in (Yang et al., 2013); or 2) the Rapamycin-binding site interacts with other parts of mTOR, which changes the catalytic rate of the enzyme and defines an allosteric inhibition mechanism (Choo et al., 2008; Yang et al., 2013). An allosteric mechanism of mTOR1 inhibition by Rapamycin is supported by modelling kinetic data on the dependence of 4EBP1 phosphorylation reaction rate on ATP concentration at different concentrations of Rapamycin (Tao et al., 2010), which shows inhibition of the catalytic rate without changing substrate affinity (Fig. 5A).

In the model, the FKPB12 protein enhances affinity of Rapamycin to the FRB domain of mTOR and does not influence substrate affinity. Note our modelling showed that the dissociation constant of complex Rapamycin-FKBP1 $K_{d,Rap2}$ differs for the substrates 4EBP1 and S6K1 (7±1.1 nM and 1.5±0.5 nM respectively) and these values correlate with their experimental IC_{50} values (9.6 nM and 2 nM respectively, Table 1). This difference may indicate steric interaction between Rapamycin-FKBP12 complex and the substrates in the model. A high affinity of Rapamycin-FKBP12 complex to the mTOR1-S6K1 complex contributes to higher inhibition of S6K1 in comparison with 4EBP1. Note, the calculation revealed high selectivity of mTOR1 to its substrates 4EBP1 and S6K1 (10.3±2 μM and 0.4±0.2 μM respectively). Additionally, mTOR1 was reported to show high selectivity to S6K isomers, S6K1 and S6K2, expressing differently in specific cells (So et al., 2016).

To juxtapose *in vitro* kinetic data for purified enzymes and *in vivo* data for cell culture we compared modelling results and experimental data on inhibition of cancer cell population by Rapamycin (Brachmann et al., 2009). Residual activity of mTOR1 (40%) relating to 4EBP1 phosphorylation obtained in the modelling correlates with survival dose dependence for a set of breast cancer cell lines treated by Everolimus (a derivative of Rapamycin) for (residual activity

is ~50%) (Brachmann et al., 2009). This fact suggests that inhibition of 4EBP1 exerts primary effect on cancer cell proliferation in comparison with S6K1 inactivation (So et al., 2016).

While a Michaelis-Menten approximation may satisfactorily describe the main features of mTOR kinetics, many kinetic properties lie out with the descriptive power of the MM approach. For example, whilst modulation of the mTOR1 activity by Rapamycin is described satisfactorily based on the kinetic properties of mTOR kinase, the inhibition of mTORC2 complex is not incompatible with the MM approximation: Rapamycin does not inhibit mTOR2 in the nanomolar concentration range (Yang et al., 2013) and a reduction in mTOR2 activity is only observed upon prolonged incubation with nanomolar rapamycin (Sarbassov et al., 2006). The mechanisms underlying this difference are presumably due to the different structural components of mTOR1 and mTOR2 complexes, including the fact that FKBP12-Rapamycin binds with a *de novo* assembled mTOR2 complex that hinders binding of Rictor components to the mTOR2 complex (Shor et al., 2008; Yang et al., 2013).

Our model does explain the Rapamycin selectivity to mTOR1 substrates S6K1 and 4EBP1 at the enzymatic level, but it is problematic to translate this on-target mechanism to *in vivo* data: Rapamycin was reported to inhibit S6K1 kinase in all cell lines that were tested, while the phosphorylation inhibition of 4EBP1 depends on cell type (Choo et al., 2008). Moreover in many cell types recovery from the initial inhibition of 4EBP1 was observed within 6 hours and was followed by its hyper-phosphorylation, which causes a recovery in cap-dependent translation despite continued S6K1 inhibition as a result of Rapamycin treatment (Choo et al., 2008). A further anomaly of mTOR kinase behaviour observed *in vivo* is that phospho-sites 4EBP1(T37/46), which are direct targets of mTOR kinases *in vitro*, are not Rapamycin sensitive *in vivo*, yet T389 on S6K1 is Rapamycin sensitive *in vitro* and *in vivo* (Choo et al., 2008).

The developed model of mTOR kinase was applied to describe the action of ATP-competitive inhibitors LY294002 and BEZ235. The dissociation constants K_d obtained in the calculation were significantly smaller than the IC_{50} values observed in *in vitro* experiments (Tao et al., 2010). To explain this difference, we used the dependence of the IC_{50} value for ATP-competitive inhibitor on ATP concentration, derived in the MM approximation. This dependence of the IC_{50} values for BEZ235 and LY294002 (Eqs. (5) and (7) respectively) describes well the observed difference between the K_d and IC_{50} values. The obtained dependence can be used to calculate the IC_{50} values for these inhibitors for different experimental assays and for the estimation of IC_{50} in *in vitro* experiments in cells with different ATP levels. These relations can be also used in the analysis of variation in the IC_{50} values for LY294002 and BEZ235 inhibitors in cancer lines characterizing by different ATP levels (Moreno-Sánchez et al., 2014; Zhou et al., 2012).

Note that according to the model of mTOR1 kinase (Eqs. (1) and (2)) and general properties of MM approximation (Brandt et al., 1987; Yung-Chi and Prusoff, 1973) the IC_{50} value for allosteric inhibitor Rapamycin does not depend on ATP concentration and its IC_{50} is equal to the dissociation constant of Rapamycin $K_{d,Rap}$ in relation to Eq. (6). This result is in agreement with experimental IC_{50} values (2 nM and 7 nM for S6K1 and 4EBP1 respectively) which are close to theoretical dissociation constants $K_{d,Rap}$ =1.5±0.5 nM and 7±1.1 nM respectively (Table 1). A comparison of dose dependencies for treatment of different cancer cell lines by rapalog, RAD001, showed that the lethal dose, $LD_{50} \cong 10$ nM (Santiskulvong et al., 2011), is almost independent of cell lines sensitive to RAD001 and satisfactorily correlates with the dissociation constant and IC_{50} values obtained in the modelling.

To investigate the joint effect of allosteric and ATP-competitive inhibitors on the mTOR kinase activity we calculated mTOR inhibition by the combination of Rapamycin and LY294002.

The result showed an additive and not a synergistic effect of this combination. Experimental data showed that a combination of Rapamycin and LY294002 suppresses AKT phosphorylation but without significant effect on treatment efficacy (Werzowa et al., 2009).

PTEN kinetics were modelled based on experimental data on PTEN activity measured in phosphatidylcholine vesicles at different molar fractions of PIP3 (McConnachie et al., 2003). We modelled PIP3 phosphatase activity of PTEN by a Michaelis-Menten equation that considered PIP3 fraction in mixed lipid vesicles. Our model is simpler than the three-parameter model used in (McConnachie et al., 2003) to describe the hopping/scooting mechanism of PTEN catalysis (see Michaelis-Menten-like equation in Table 3). In this model, the maximum reaction rate depends on the surface fraction of PIP3 in the vesicle membrane, and the rate equation takes into account non-specific binding of PTEN to the membrane surface with low affinity, K_S =84 mM (McConnachie et al., 2003). In our model we showed that experimental PTEN kinetics might be satisfactory described in Michaelis-Menten approximation where the maximum reaction rate does not depend on molar fraction of PIP3 in the membrane and that the reaction occurs through the formation of Michaelis-Menten enzyme-substrate complex without non-specific binding of PTEN to the membrane. Our model gave a low Michaelis constant K_{PIP3}=43 nM that suggests that PTEN is highly sensitive to low concentrations of PIP3 lipids produced in the plasma membrane during PI3K activation (Maehama et al., 2001).

Here, our modelling and obtained results show that integrated analysis of experimental data on enzymatic kinetics, enzyme activity following drug action, and enzyme molecular structure gives mutually complementary information on regulation mechanisms of catalysis and mechanisms of inhibitor action in various experimental conditions. Our framework provides an approach to integrate protein and drug data into a unified, validated kinetic model that may be used to predict drug efficacy in a range of cellular conditions.

Conflict of interest

The authors report no conflict of interest.

Acknowledgments

This work was supported by grants from The Northwood Trust (AG, JB), and personal support to AG from Scottish Informatics and Computer Science Alliance (SICSA). We also acknowledge reviewers whom comments significantly improved the article.

References

Acker, M.G., Auld, D.S., 2014. Considerations for the design and reporting of enzyme assays in high-throughput screening applications. Perspectives in Science 1, 56–73. doi:10.1016/j.pisc.2013.12.001

Banaszynski, L.A., Liu, C.W., Wandless, T.J., 2005. Characterization of the FKBP.rapamycin.FRB ternary complex. Journal of the American Chemical Society 127, 4715–21. doi:10.1021/ja043277y

Bendell, J.C., Kurkjian, C., Infante, J.R., Bauer, T.M., Burris, H.A., Greco, F.A., Shih, K.C., Thompson, D.S., Lane, C.M., Finney, L.H., Jones, S.F., 2015. A phase 1 study of the sachet formulation of the oral dual PI3K/mTOR inhibitor BEZ235 given twice daily (BID) in patients with advanced solid tumors. Investigational new drugs 33, 463–71.

doi:10.1007/s10637-015-0218-6

Brachmann, S.M., Hofmann, I., Schnell, C., Fritsch, C., Wee, S., Lane, H., Wang, S., Garcia-Echeverria, C., Maira, S.-M., 2009. Specific apoptosis induction by the dual PI3K/mTor inhibitor NVP-BEZ235 in HER2 amplified and PIK3CA mutant breast cancer cells. Proceedings of the National Academy of Sciences of the United States of America 106, 22299–304. doi:10.1073/pnas.0905152106

Brandt, R.B., Laux, J.E., Yates, S.W., 1987. Calculation of inhibitor Ki and inhibitor type from the concentration of inhibitor for 50% inhibition for Michaelis-Menten enzymes. Biochemical Medicine and Metabolic Biology 37, 344–349. doi:10.1016/0885-4505(87)90046-6

Chandarlapaty, S., 2012. Negative feedback and adaptive resistance to the targeted therapy of cancer. Cancer discovery 2, 311–9. doi:10.1158/2159-8290.CD-12-0018

Choo, A.Y., Yoon, S.-O., Kim, S.G., Roux, P.P., Blenis, J., 2008. Rapamycin differentially inhibits S6Ks and 4E-BP1 to mediate cell-type-specific repression of mRNA translation. Proceedings of the National Academy of Sciences of the United States of America 105, 17414–9. doi:10.1073/pnas.0809136105

Cornish-Bowden, A., 2014. Analysis and interpretation of enzyme kinetic data. Perspectives in Science 1, 121–125. doi:10.1016/j.pisc.2014.02.010

Cornish-Bowden, A., 2013. The origins of enzyme kinetics. FEBS letters 587, 2725–30. doi:10.1016/j.febslet.2013.06.009

Cornish-Bowden, A., 2004. Fundamentals of Enzyme Kinetics (3rd Edition), Portland Press Ltd.

Cully, M., You, H., Levine, A.J., Mak, T.W., 2006. Beyond PTEN mutations: the PI3K pathway as an integrator of multiple inputs during tumorigenesis. Nature reviews. Cancer 6, 184–92. doi:10.1038/nrc1819

Cvijovic, M., Almquist, J., Hagmar, J., Hohmann, S., Kaltenbach, H.-M., Klipp, E., Krantz, M., Mendes, P., Nelander, S., Nielsen, J., Pagnani, A., Przulj, N., Raue, A., Stelling, J., Stoma, S., Tobin, F., Wodke, J.A.H., Zecchina, R., Jirstrand, M., 2014. Bridging the gaps in systems biology. Molecular genetics and genomics : MGG 289, 727–34. doi:10.1007/s00438-014-0843-3

Demin, O., Goryanin, I., 2008. Kinetic Modelling in Systems Biology - CRC Press Book [WWW Document]. Taylor and Francis. URL https://www.crcpress.com/Kinetic-Modelling-in-Systems-Biology/Demin-Goryanin/9781584886679 (accessed 3.31.16).

Draper, N.R., Smith, H., 2014. Applied Regression Analysis, 3rd Edition [WWW Document]. John Wiley & Sons. URL http://eu.wiley.com/WileyCDA/WileyTitle/productCd-0471170828.html (accessed 4.14.16).

Efron, B., Tibshirani, R., 1994. An introduction to the bootstrap. Chapman & Hall.

Gharbi, S.I., Zvelebil, M.J., Shuttleworth, S.J., Hancox, T., Saghir, N., Timms, J.F., Waterfield, M.D., 2007. Exploring the specificity of the PI3K family inhibitor LY294002. The Biochemical journal 404, 15–21. doi:10.1042/BJ20061489

Goltsov, A., Faratian, D., Langdon, S.P., Mullen, P., Harrison, D.J., Bown, J., 2012. Features of the reversible sensitivity-resistance transition in PI3K/PTEN/AKT signalling network after HER2 inhibition. Cellular Signalling 24, 493–504. doi:10.1016/j.cellsig.2011.09.030

Goryachev, A.B., Pokhilko, A. V, 2006. Computational model explains high activity and rapid

cycling of Rho GTPases within protein complexes. PLoS computational biology 2, e172. doi:10.1371/journal.pcbi.0020172

Harrington, L.S., Findlay, G.M., Gray, A., Tolkacheva, T., Wigfield, S., Rebholz, H., Barnett, J., Leslie, N.R., Cheng, S., Shepherd, P.R., Gout, I., Downes, C.P., Lamb, R.F., 2004. The TSC1-2 tumor suppressor controls insulin-PI3K signaling via regulation of IRS proteins. The Journal of cell biology 166, 213–23. doi:10.1083/jcb.200403069

Hassan, B., Akcakanat, A., Sangai, T., Evans, K.W., Adkins, F., Eterovic, A.K., Zhao, H., Chen, K., Chen, H., Do, K.-A., Xie, S.M., Holder, A.M., Naing, A., Mills, G.B., Meric-Bernstam, F., 2014. Catalytic mTOR inhibitors can overcome intrinsic and acquired resistance to allosteric mTOR inhibitors. Oncotarget 5, 8544–57.

Huang, W., Jiang, D., Wang, X., Wang, K., Sims, C.E., Allbritton, N.L., Zhang, Q., 2011. Kinetic analysis of PI3K reactions with fluorescent PIP2 derivatives. Analytical and bioanalytical chemistry 401, 1881–8. doi:10.1007/s00216-011-5257-z

Hudes, G., Carducci, M., Tomczak, P., Dutcher, J., Figlin, R., Kapoor, A., Staroslawska, E., Sosman, J., McDermott, D., Bodrogi, I., Kovacevic, Z., Lesovoy, V., Schmidt-Wolf, I.G.H., Barbarash, O., Gokmen, E., O'Toole, T., Lustgarten, S., Moore, L., Motzer, R.J., 2007. Temsirolimus, interferon alfa, or both for advanced renal-cell carcinoma. The New England journal of medicine 356, 2271–81. doi:10.1056/NEJMoa066838

Jacinto, E., Loewith, R., Schmidt, A., Lin, S., Rüegg, M.A., Hall, A., Hall, M.N., 2004. Mammalian TOR complex 2 controls the actin cytoskeleton and is rapamycin insensitive. Nature cell biology 6, 1122–8. doi:10.1038/ncb1183

Jebahi, A., Villedieu, M., Pétigny-Lechartier, C., Brotin, E., Louis, M.-H., Abeilard, E., Giffard, F., Guercio, M., Briand, M., Gauduchon, P., Lheureux, S., Poulain, L., 2014. PI3K/mTOR dual inhibitor NVP-BEZ235 decreases Mcl-1 expression and sensitizes ovarian carcinoma cells to Bcl-xL-targeting strategies, provided that Bim expression is induced. Cancer letters 348, 38–49. doi:10.1016/j.canlet.2014.03.001

Kalachand, R., Hennessy, B.T., Markman, M., 2011. Molecular targeted therapy in ovarian cancer: what is on the horizon? Drugs 71, 947–67. doi:10.2165/11591740-000000000-00000

Keshwani, M.M., Harris, T.K., 2008. Kinetic mechanism of fully activated S6K1 protein kinase. The Journal of biological chemistry 283, 11972–80. doi:10.1074/jbc.M800114200

Laplante, M., Sabatini, D.M., 2012. mTOR signaling in growth control and disease. Cell 149, 274–93. doi:10.1016/j.cell.2012.03.017

Maehama, T., Taylor, G.S., Dixon, J.E., 2001. PTEN and myotubularin: novel phosphoinositide phosphatases. Annual review of biochemistry 70, 247–79. doi:10.1146/annurev.biochem.70.1.247

Maira, S.-M., Stauffer, F., Brueggen, J., Furet, P., Schnell, C., Fritsch, C., Brachmann, S., Chène, P., De Pover, A., Schoemaker, K., Fabbro, D., Gabriel, D., Simonen, M., Murphy, L., Finan, P., Sellers, W., García-Echeverría, C., 2008. Identification and characterization of NVP-BEZ235, a new orally available dual phosphatidylinositol 3-kinase/mammalian target of rapamycin inhibitor with potent in vivo antitumor activity. Molecular cancer therapeutics 7, 1851–63. doi:10.1158/1535-7163.MCT-08-0017

Markman, B., Dienstmann, R., Tabernero, J., 2010. Targeting the PI3K/Akt/mTOR pathway--

beyond rapalogs. Oncotarget 1, 530–43. doi:10.18632/oncotarget.101012

McConnachie, G., Pass, I., Walker, S.M., Downes, C.P., 2003. Interfacial kinetic analysis of the tumour suppressor phosphatase, PTEN: evidence for activation by anionic phospholipids. The Biochemical journal 371, 947–55. doi:10.1042/BJ20021848

McLaughlin, S., Wang, J., Gambhir, A., Murray, D., 2002. PIP(2) and proteins: interactions, organization, and information flow. Annual review of biophysics and biomolecular structure 31, 151–75. doi:10.1146/annurev.biophys.31.082901.134259

Metelkin, E., Demin, O., Kovács, Z., Chinopoulos, C., 2009. Modeling of ATP-ADP steady-state exchange rate mediated by the adenine nucleotide translocase in isolated mitochondria. The FEBS journal 276, 6942–55. doi:10.1111/j.1742-4658.2009.07394.x

Mita, M., Mita, A., Rowinsky, E.K. (Eds.), 2016. mTOR Inhibition for Cancer Therapy: Past, Present and Future, 1st ed. Springer.

Moreno-Sánchez, R., Marín-Hernández, A., Saavedra, E., Pardo, J.P., Ralph, S.J., Rodríguez-Enríquez, S., 2014. Who controls the ATP supply in cancer cells? Biochemistry lessons to understand cancer energy metabolism. The international journal of biochemistry & cell biology 50, 10–23. doi:10.1016/j.biocel.2014.01.025

Nik-Zainal, S., Davies, H., Staaf, J., Ramakrishna, M., Glodzik, D., Zou, X., Martincorena, I., Alexandrov, L.B., Martin, S., Wedge, D.C., Van Loo, P., Ju, Y.S., Smid, M., Brinkman, A.B., Morganella, S., Aure, M.R., Lingjærde, O.C., Langerød, A., Ringnér, M., Ahn, S.-M., Boyault, S., Brock, J.E., Broeks, A., Butler, A., Desmedt, C., Dirix, L., Dronov, S., Fatima, A., Foekens, J.A., Gerstung, M., Hooijer, G.K.J., Jang, S.J., Jones, D.R., Kim, H.-Y., King, T.A., Krishnamurthy, S., Lee, H.J., Lee, J.-Y., Li, Y., McLaren, S., Menzies, A., Mustonen, V., O'Meara, S., Pauporté, I., Pivot, X., Purdie, C.A., Raine, K., Ramakrishnan, K., Rodríguez-González, F.G., Romieu, G., Sieuwerts, A.M., Simpson, P.T., Shepherd, R., Stebbings, L., Stefansson, O.A., Teague, J., Tommasi, S., Treilleux, I., Van den Eynden, G.G., Vermeulen, P., Vincent-Salomon, A., Yates, L., Caldas, C., Veer, L. van't, Tutt, A., Knappskog, S., Tan, B.K.T., Jonkers, J., Borg, Å., Ueno, N.T., Sotiriou, C., Viari, A., Futreal, P.A., Campbell, P.J., Span, P.N., Van Laere, S., Lakhani, S.R., Eyfjord, J.E., Thompson, A.M., Birney, E., Stunnenberg, H.G., van de Vijver, M.J., Martens, J.W.M., Børresen-Dale, A.-L., Richardson, A.L., Kong, G., Thomas, G., Stratton, M.R., 2016. Landscape of somatic mutations in 560 breast cancer whole-genome sequences. Nature advance on. doi:10.1038/nature17676

Santiskulvong, C., Konecny, G.E., Fekete, M., Chen, K.-Y.M., Karam, A., Mulholland, D., Eng, C., Wu, H., Song, M., Dorigo, O., 2011. Dual targeting of phosphoinositide 3-kinase and mammalian target of rapamycin using NVP-BEZ235 as a novel therapeutic approach in human ovarian carcinoma. Clinical cancer research : an official journal of the American Association for Cancer Research 17, 2373–84. doi:10.1158/1078-0432.CCR-10-2289

Sarbassov, D.D., Ali, S.M., Sengupta, S., Sheen, J.-H., Hsu, P.P., Bagley, A.F., Markhard, A.L., Sabatini, D.M., 2006. Prolonged rapamycin treatment inhibits mTORC2 assembly and Akt/PKB. Molecular cell 22, 159–68. doi:10.1016/j.molcel.2006.03.029

Schnell, S., 2014. Validity of the Michaelis-Menten equation--steady-state or reactant stationary assumption: that is the question. The FEBS journal 281, 464–72. doi:10.1111/febs.12564

Serra, V., Markman, B., Scaltriti, M., Eichhorn, P.J.A., Valero, V., Guzman, M., Botero, M.L., Llonch, E., Atzori, F., Di Cosimo, S., Maira, M., Garcia-Echeverria, C., Parra, J.L., Arribas, J.,

Baselga, J., 2008. NVP-BEZ235, a dual PI3K/mTOR inhibitor, prevents PI3K signaling and inhibits the growth of cancer cells with activating PI3K mutations. Cancer research 68, 8022–30. doi:10.1158/0008-5472.CAN-08-1385

Shoji, K., Oda, K., Kashiyama, T., Ikeda, Y., Nakagawa, S., Sone, K., Miyamoto, Y., Hiraike, H., Tanikawa, M., Miyasaka, A., Koso, T., Matsumoto, Y., Wada-Hiraike, O., Kawana, K., Kuramoto, H., McCormick, F., Aburatani, H., Yano, T., Kozuma, S., Taketani, Y., 2012. Genotype-dependent efficacy of a dual PI3K/mTOR inhibitor, NVP-BEZ235, and an mTOR inhibitor, RAD001, in endometrial carcinomas. PloS one 7, e37431. doi:10.1371/journal.pone.0037431

Shor, B., Zhang, W.-G., Toral-Barza, L., Lucas, J., Abraham, R.T., Gibbons, J.J., Yu, K., 2008. A new pharmacologic action of CCI-779 involves FKBP12-independent inhibition of mTOR kinase activity and profound repression of global protein synthesis. Cancer research 68, 2934–43. doi:10.1158/0008-5472.CAN-07-6487

Siddiqui, N., Sonenberg, N., 2015. Signalling to eIF4E in cancer. Biochemical Society transactions 43, 763–72. doi:10.1042/BST20150126

So, L., Lee, J., Palafox, M., Mallya, S., Woxland, C.G., Arguello, M., Truitt, M.L., Sonenberg, N., Ruggero, D., Fruman, D.A., 2016. The 4E-BP-eIF4E axis promotes rapamycin-sensitive growth and proliferation in lymphocytes. Science signaling 9, ra57. doi:10.1126/scisignal.aad8463

Stemke-Hale, K., Gonzalez-Angulo, A.M., Lluch, A., Neve, R.M., Kuo, W.-L., Davies, M., Carey, M., Hu, Z., Guan, Y., Sahin, A., Symmans, W.F., Pusztai, L., Nolden, L.K., Horlings, H., Berns, K., Hung, M.-C., van de Vijver, M.J., Valero, V., Gray, J.W., Bernards, R., Mills, G.B., Hennessy, B.T., 2008. An integrative genomic and proteomic analysis of PIK3CA, PTEN, and AKT mutations in breast cancer. Cancer research 68, 6084–91. doi:10.1158/0008-5472.CAN-07-6854

Tao, Z., Barker, J., Shi, S.D.-H., Gehring, M., Sun, S., 2010. Steady-state kinetic and inhibition studies of the mammalian target of rapamycin (mTOR) kinase domain and mTOR complexes. Biochemistry 49, 8488–98. doi:10.1021/bi100673c

Toral-Barza, L., Zhang, W.-G., Lamison, C., Larocque, J., Gibbons, J., Yu, K., 2005. Characterization of the cloned full-length and a truncated human target of rapamycin: activity, specificity, and enzyme inhibition as studied by a high capacity assay. Biochemical and biophysical research communications 332, 304–10. doi:10.1016/j.bbrc.2005.04.117

Tummler, K., Lubitz, T., Schelker, M., Klipp, E., 2014. New types of experimental data shape the use of enzyme kinetics for dynamic network modeling. The FEBS journal 281, 549–71. doi:10.1111/febs.12525

Vlahos, C.J., Matter, W.F., Hui, K.Y., Brown, R.F., 1994. A specific inhibitor of phosphatidylinositol 3-kinase, 2-(4-morpholinyl)-8-phenyl-4H-1-benzopyran-4-one (LY294002). The Journal of biological chemistry 269, 5241–8.

Walker, E.H., Pacold, M.E., Perisic, O., Stephens, L., Hawkins, P.T., Wymann, M.P., Williams, R.L., 2000. Structural Determinants of Phosphoinositide 3-Kinase Inhibition by Wortmannin, LY294002, Quercetin, Myricetin, and Staurosporine. Molecular Cell 6, 909–919. doi:10.1016/S1097-2765(05)00089-4

Wang, C.-C., Cirit, M., Haugh, J.M., 2009. PI3K-dependent cross-talk interactions converge with Ras as quantifiable inputs integrated by Erk. Molecular systems biology 5, 246. doi:10.1038/msb.2009.4

Werzowa, J., Cejka, D., Fuereder, T., Dekrout, B., Thallinger, C., Pehamberger, H., Wacheck, V., Pratscher, B., 2009. Suppression of mTOR complex 2-dependent AKT phosphorylation in melanoma cells by combined treatment with rapamycin and LY294002. The British journal of dermatology 160, 955–64. doi:10.1111/j.1365-2133.2008.08991.x

Yang, H., Rudge, D.G., Koos, J.D., Vaidialingam, B., Yang, H.J., Pavletich, N.P., 2013. mTOR kinase structure, mechanism and regulation. Nature 497, 217–23. doi:10.1038/nature12122

Yu, Y., Yoon, S.-O., Poulogiannis, G., Yang, Q., Ma, X.M., Villen, J., Kubica, N., Hoffman, G.R., Cantley, L.C., Gygi, S.P., Blenis, J., 2011. Phosphoproteomic Analysis Identifies Grb10 as an mTORC1 Substrate That Negatively Regulates Insulin Signaling. Science 332, 1322–1326. doi:10.1126/science.1199484

Yung-Chi, C., Prusoff, W.H., 1973. Relationship between the inhibition constant (KI) and the concentration of inhibitor which causes 50 per cent inhibition (I50) of an enzymatic reaction. Biochemical Pharmacology 22, 3099–3108. doi:10.1016/0006-2952(73)90196-2

Zhou, Y., Tozzi, F., Chen, J., Fan, F., Xia, L., Wang, J., Gao, G., Zhang, A., Xia, X., Brasher, H., Widger, W., Ellis, L.M., Weihua, Z., 2012. Intracellular ATP levels are a pivotal determinant of chemoresistance in colon cancer cells. Cancer research 72, 304–14. doi:10.1158/0008-5472.CAN-11-1674

Zoncu, R., Efeyan, A., Sabatini, D.M., 2011. mTOR: from growth signal integration to cancer, diabetes and ageing. Nature reviews. Molecular cell biology 12, 21–35. doi:10.1038/nrm3025

Figure legends

Fig. 1. Scheme of PI3K/PTEN/AKT/mTOR1 pathway activated by growth factor (GF) and inhibited by allosteric inhibitor, Rapamycin, and ATP-competitive inhibitors BEZ235 and LY294002.

Fig. 2. Systems biology approach to kinetic model design, discrimination, and calibration: incorporation and fitting of *in vitro* data obtained under different experimental conditions. Application of the model to the prediction of IC_{50} values for drugs in different *in vitro* and *in vivo* conditions.

Fig. 3. Catalytic cycle of mTOR1 complex catalysing the reactions of S6K1 and 4EBP1 phosphorylation in the presence of ATP-competitive inhibitors (Inh) either BEZ235 or LY294002 and allosteric inhibitor Rapamycin (Rap).

Fig. 4. Catalytic cycle of PI3K in the presence of ATP-competitive inhibitors, BEZ235 and LY294002.

Fig. 5. (A): Reaction rate of 4EBP1(Thr46) phosphorylation catalysed by mTOR kinase depending on ATP concentration at different concentrations of Rapamycin. Lines - theoretical results: line 1 - 0 nM, line 2 – 8 nM, line 3 – 20 nM, line 4 – 128 nM. Points - experimental data: 200 nM 4EBP1, 3 nM truncated mammalian mTOR kinase, 200 nM FKBP12 protein in TR-FRET assay (Tao et al., 2010). (B): Reaction rate of 4EBP1(Thr46) phosphorylation catalysed by mTOR kinase depending on 4EBP1 concentration. Line - theoretical result. Points - experimental data: 300 μM ATP, 6.7 nM truncated mammalian mTOR kinase in radiometric filtration assay (Tao et al., 2010). (C): Dose dependence of mTOR1 reaction rate inhibition by Rapamycin (line 1) and BEZ235 (line 2). Lines – theoretical results. Points - experimental data: 40 μM 4EBP1, 20 nM mammalian mTOR1, and 100 μM ATP in radiometric filtration assay (Tao et al., 2010).

Fig. 6. (A): Dependence of mTOR1 reaction rate of S6K1(Thr389) phosphorylation on ATP concentration at different concentrations of LY294002 inhibitor. Lines - theoretical results: line 1 - 0 μM, line 2 - 0.8 μM, line 3 - 1.6 μM, and line 4 - 3.2 μM LY294002. Points - experimental data: 1.25 μM S6K1, ATP 100 μM, 6 nM FLAG-TOR in the assay (Toral-Barza et al., 2005). (B): Dose dependence of mTOR kinase reaction rate of S6K1(Thr389) phosphorylation on Rapamycin concentration in the presence (line 1) and absence of FKBP12 (line 2). Lines -theoretical results. Points - experimental data: circles and triangles (Toral-Barza et al., 2005), squares (Shor et al., 2008). Experimental conditions: 1.25 μM S6K1, 6 nM FLAG-TOR, and 100 μM ATP in the assay. (C): Dose dependence of inhibition of FLAG-TOR(3.5) reaction rate of S6K1(Thr389) phosphorylation by LY294002. Lines 1 and 2 - theoretical calculation at 100 μM and 2 μM ATP, respectively. Points - experimental data: 1.25 μM S6K1, 100 μM ATP, 6 nM FLAG-TOR(3.5) in the assay (Toral-Barza et al., 2005). Line 3 - computational dose dependence of inhibition of mTOR kinase by combination of LY294002 and Rapamycin (10 nM) at 100 μM ATP.

Fig. 7. (A): The dependence of PI3K reaction rate on ATP concentration. Line – theoretical result. Points - experimental data: 2 μM PIP2 in the assay (Huang et al., 2011). (B): The dose dependence of PI3K reaction rate on PIP2 concentration. Line – theoretical result. Points - experimental data: 2 mM ATP in the assay (Huang et al., 2011). (C): Lineweaver-Burk plot of

PI3K reaction rate for different LY294002 concentrations: line 1 - 0 μM, line 2 - 1 μM, line 3 - 5μM, line 4 - 10 μM, and line 5 - 20 μM LY294002. Lines – theoretical results. Points - experimental data: 400 μM PIP2 in the assay (Vlahos et al., 1994). (D): Dose dependence of ADP production inhibition on BEZ235 (line 1) and LY294002 (line 2) concentrations. Lines - theoretical calculations, points - experimental data on the inhibition of ADP production by PI3Kα (p85/p110α complex) on BEZ235 (circles) and LY294002 (squares) concentrations: 0.5 μATP, 10 μM PIP2, 0.4 μg/mL PI3Kα, time of reaction stopping t=60 min in the ADP-release assay (Maira et al., 2008).

Fig. 8. Dependence of IC_{50} for BEZ235 (A) and LY294002 (B) for PI3K on ATP concentration obtained based on dose dependence of ADP production on inhibitor concentration. Lines – theoretical IC_{50} dependencies for ADP production calculated according to Eq. (9) (solid lines) and for the reaction rate calculated by Eqs. (5) and (7) (dotted lines). Points - experimental data for PI3Kγ: 10 μM PIP2, 10 nM PI3Kα in the assay, reaction was terminated after t_m=120 min (Maira et al., 2008).

Fig. 9. Dependence of reaction rate of PIP3 hydrolysis by PTEN on PIP3 concentration at the different molar fractions of PIP3, X_{PIP3} given in reciprocal axes $1/V_{PTEN}$ and $1/PIP3$. Lines - theoretical results, points - experimental data on PTEN activity measured in phosphatidilcholin vesicles at X_{PIP3}=0.1 (filled circle, line 1), 0.01 (open circles, line 2), 0.002 (filled squares, line 3), and 0.001 (open squares, line 4) (McConnachie et al., 2003).

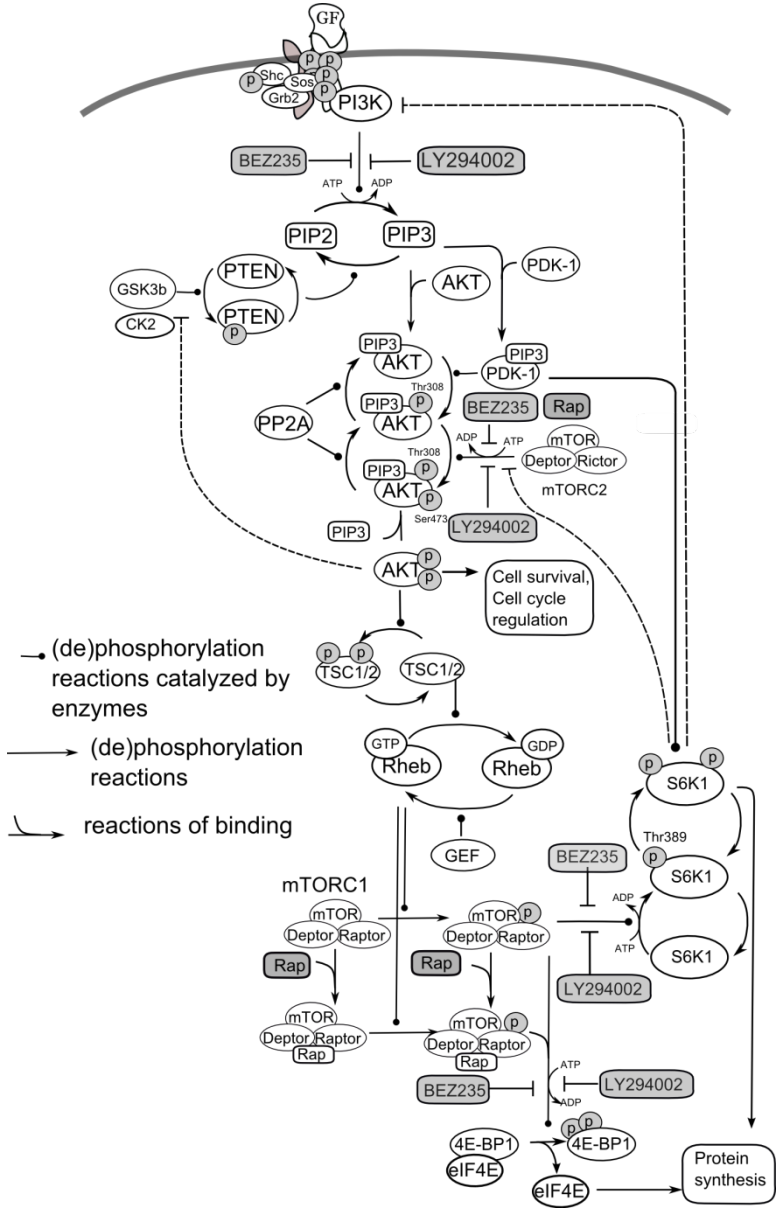
GF
Shc
Sos
Grb2
PI3K
BEZ235
LY294002
ATP
ADP
PIP2
PIP3
PDK-1
AKT
PTEN
GSK3b
CK2
PP2A
Thr308
Ser473
mTOR
Deptor
Rictor
mTORC2
Rap
Cell survival,
Cell cycle
regulation
TSC1/2
GTP
GDP
Rheb
GEF
S6K1
Thr389
mTORC1
Raptor
4E-BP1
eIF4E
Protein
synthesis
(de)phosphorylation reactions catalyzed by enzymes
(de)phosphorylation reactions
reactions of binding

Fig. 1.

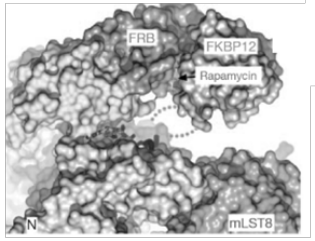

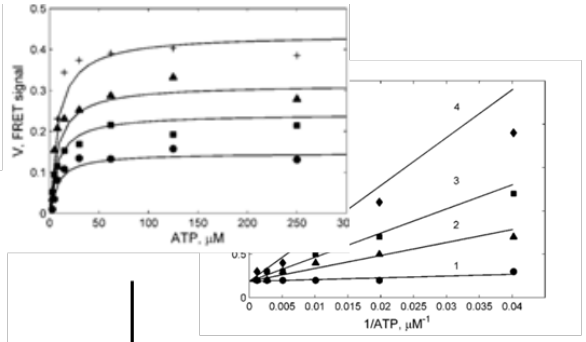

Experimental data on enzyme kinetics in different *in vitro* assays

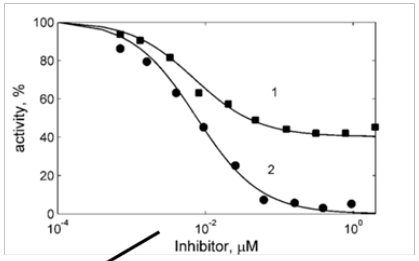

Molecular structure of enzyme–substrate and enzyme-inhibitor complexes

Kinetic model designing and calibration

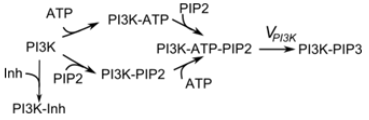

$$\frac{dP}{dt} = V$$

Dose dependencies of enzyme activity on drug concentration in different *in vitro* assays

Calibrated kinetic model of the enzyme

Kinetic parameters of enzyme and inhibitors

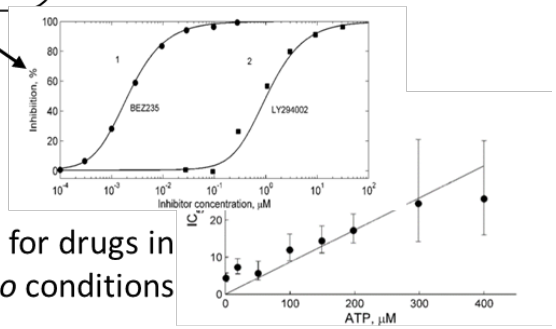

Prediction of IC_{50} values for drugs in different *in vitro* and *in vivo* conditions

Fig. 2.

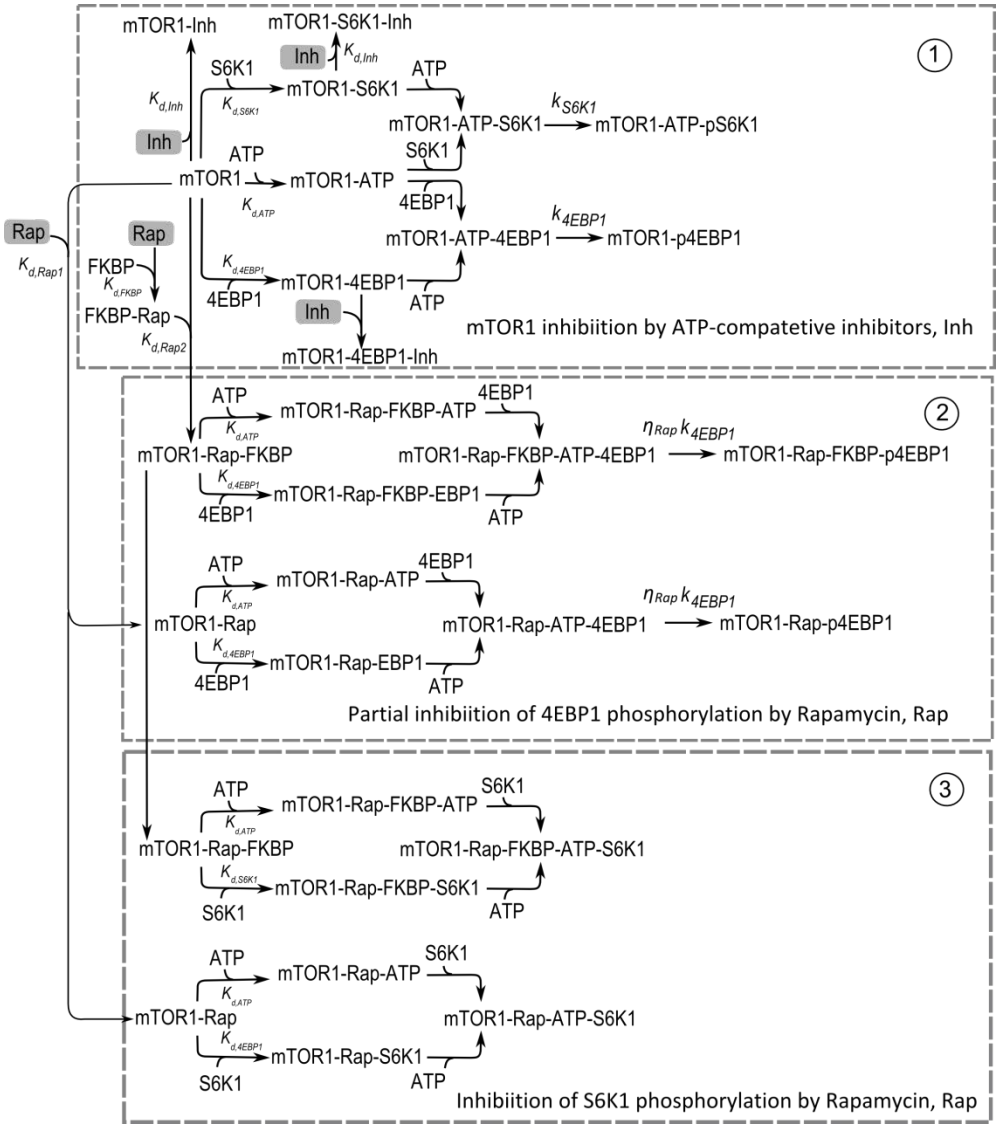
mTOR1-Inh
mTOR1-S6K1-Inh
Inh
$K_{d,Inh}$
S6K1
$K_{d,S6K1}$
mTOR1-S6K1
ATP
mTOR1-ATP-S6K1
k_{S6K1}
mTOR1-ATP-pS6K1
mTOR1
mTOR1-ATP
$K_{d,ATP}$
4EBP1
mTOR1-ATP-4EBP1
k_{4EBP1}
mTOR1-p4EBP1
Rap
$K_{d,Rap1}$
FKBP
$K_{d,FKBP}$
FKBP-Rap
$K_{d,Rap2}$
$K_{d,4EBP1}$
mTOR1-4EBP1
mTOR1-4EBP1-Inh
mTOR1 inhibiition by ATP-compatetive inhibitors, Inh
mTOR1-Rap-FKBP-ATP
mTOR1-Rap-FKBP-ATP-4EBP1
$\eta_{Rap} k_{4EBP1}$
mTOR1-Rap-FKBP-p4EBP1
mTOR1-Rap-FKBP-EBP1
mTOR1-Rap-ATP
mTOR1-Rap-ATP-4EBP1
mTOR1-Rap-p4EBP1
mTOR1-Rap-EBP1
Partial inhibiition of 4EBP1 phosphorylation by Rapamycin, Rap
mTOR1-Rap-FKBP-S6K1
mTOR1-Rap-FKBP-ATP-S6K1
mTOR1-Rap-ATP-S6K1
mTOR1-Rap-S6K1
Inhibiition of S6K1 phosphorylation by Rapamycin, Rap

Fig. 3

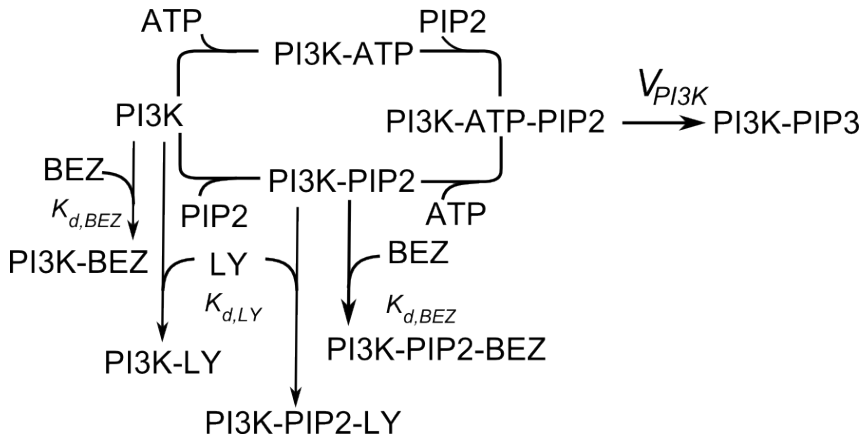
ATP
PIP2
PI3K-ATP
PI3K
PI3K-ATP-PIP2
V_{PI3K}
PI3K-PIP3
BEZ
$K_{d,BEZ}$
PI3K-PIP2
PIP2
ATP
PI3K-BEZ
LY
$K_{d,LY}$
BEZ
$K_{d,BEZ}$
PI3K-LY
PI3K-PIP2-BEZ
PI3K-PIP2-LY

Fig. 4.

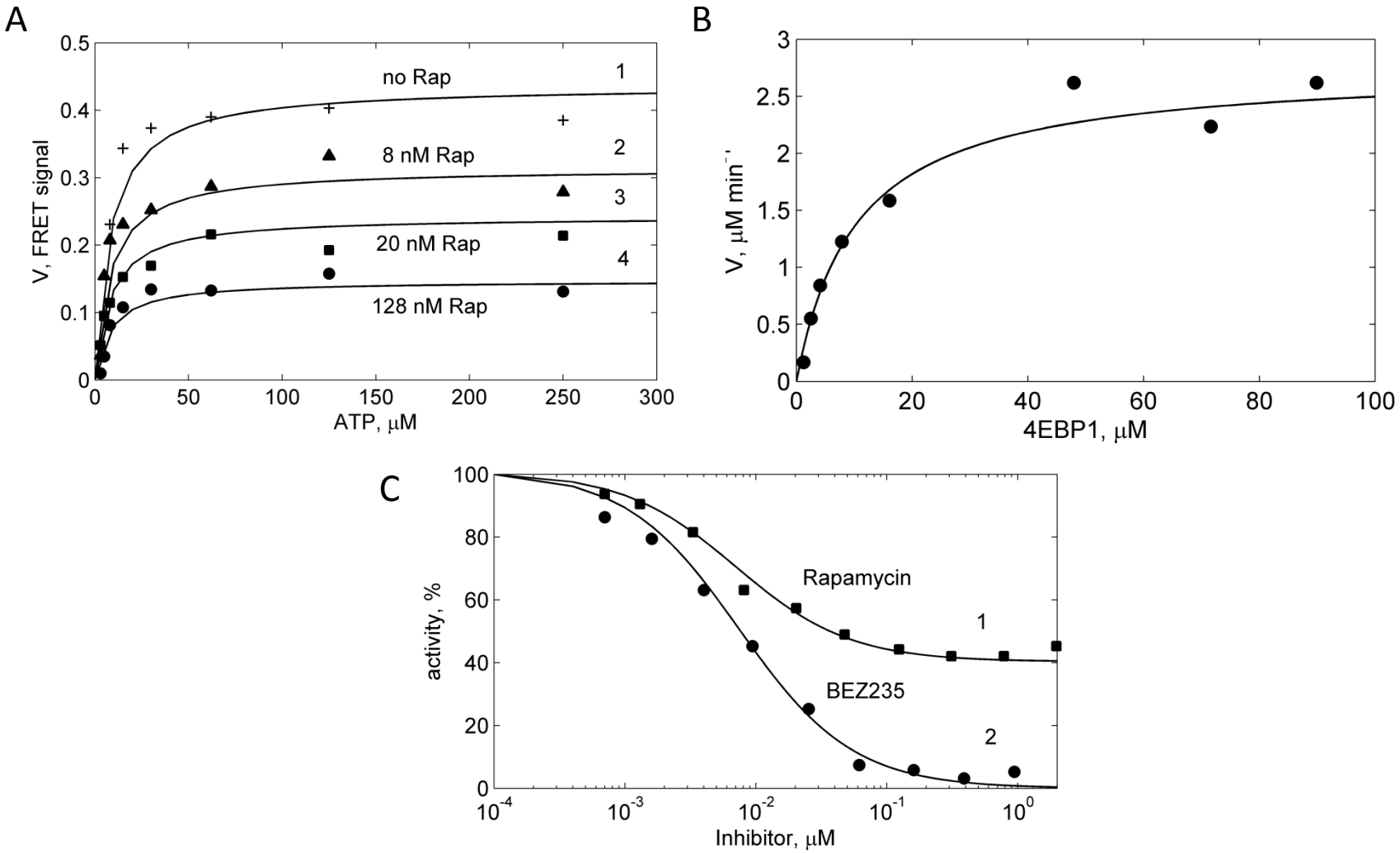
A
V, FRET signal
ATP, μM
no Rap
1
8 nM Rap
2
20 nM Rap
3
128 nM Rap
4
B
V, μM min⁻¹
4EBP1, μM
C
activity, %
Inhibitor, μM
Rapamycin
1
BEZ235
2

Fig. 5.

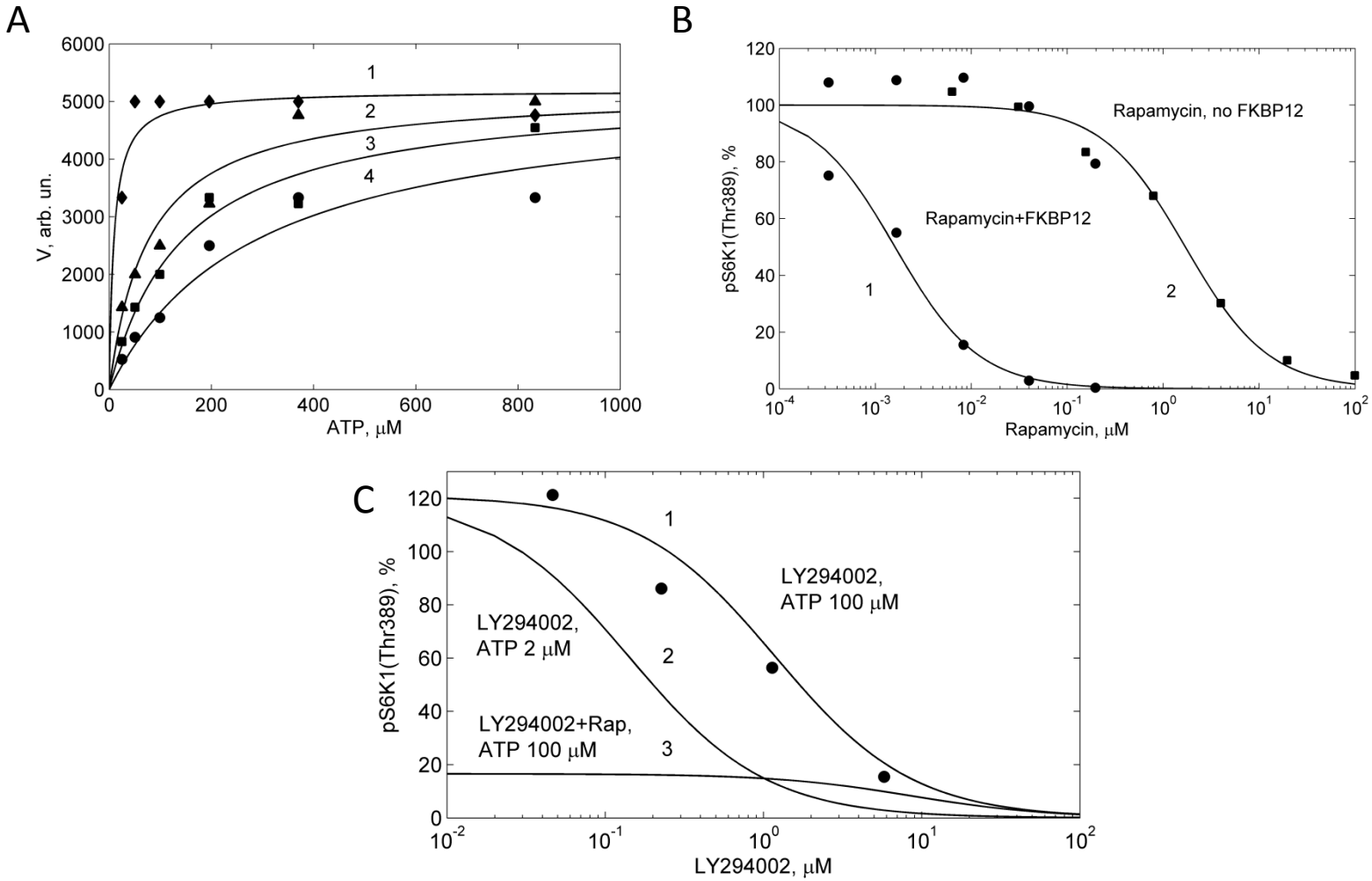
A
V, arb. un.
ATP, μM
1
2
3
4
B
pS6K1(Thr389), %
Rapamycin, μM
Rapamycin, no FKBP12
Rapamycin+FKBP12
1
2
C
pS6K1(Thr389), %
LY294002, μM
LY294002,
ATP 100 μM
LY294002,
ATP 2 μM
LY294002+Rap,
ATP 100 μM
1
2
3

Fig. 6.

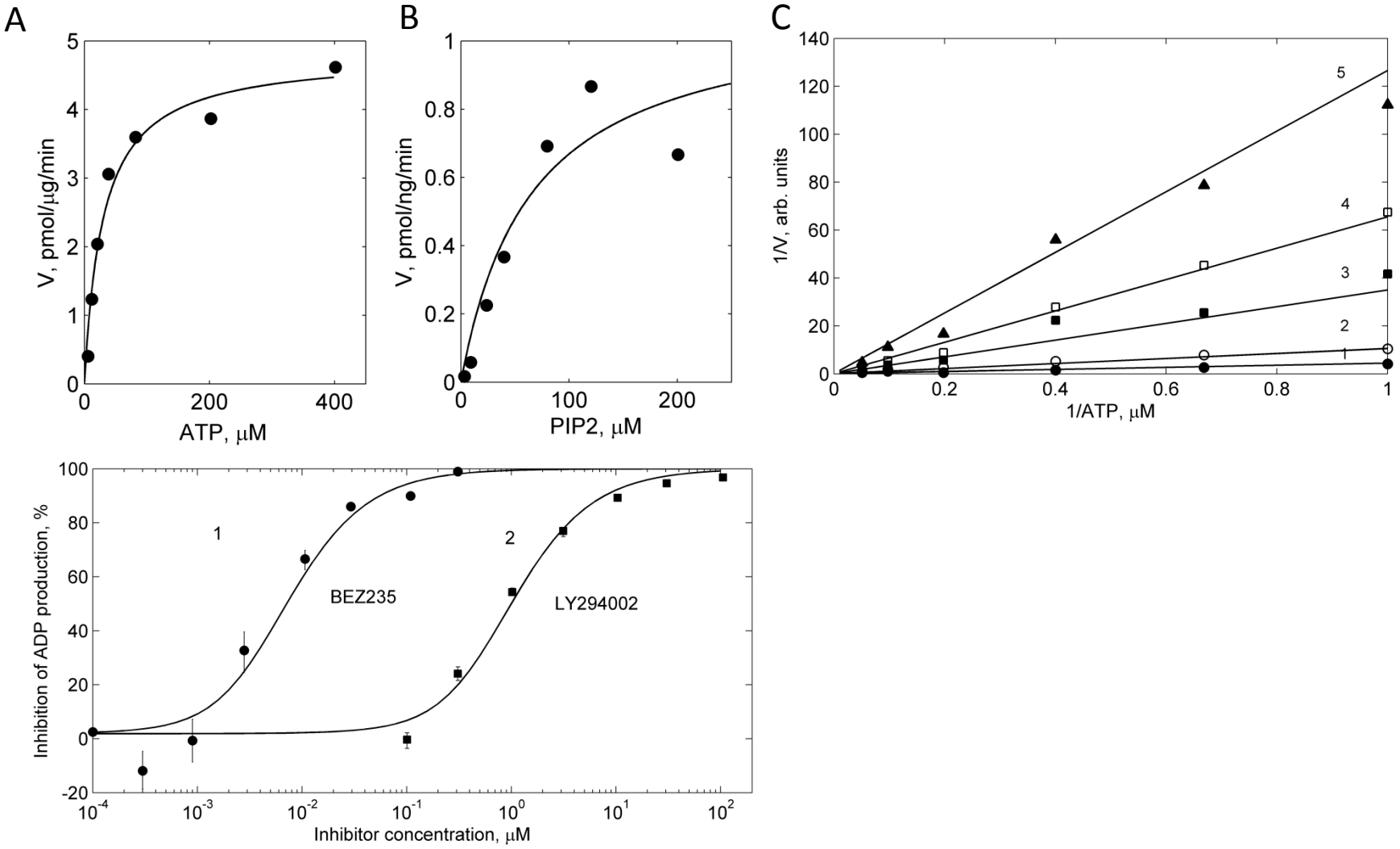
A
V, pmol/μg/min
ATP, μM
B
V, pmol/ng/min
PIP2, μM
C
1/V, arb. units
1/ATP, μM
5
4
3
2
D
Inhibition of ADP production, %
Inhibitor concentration, μM
1
BEZ235
2
LY294002

Fig. 7

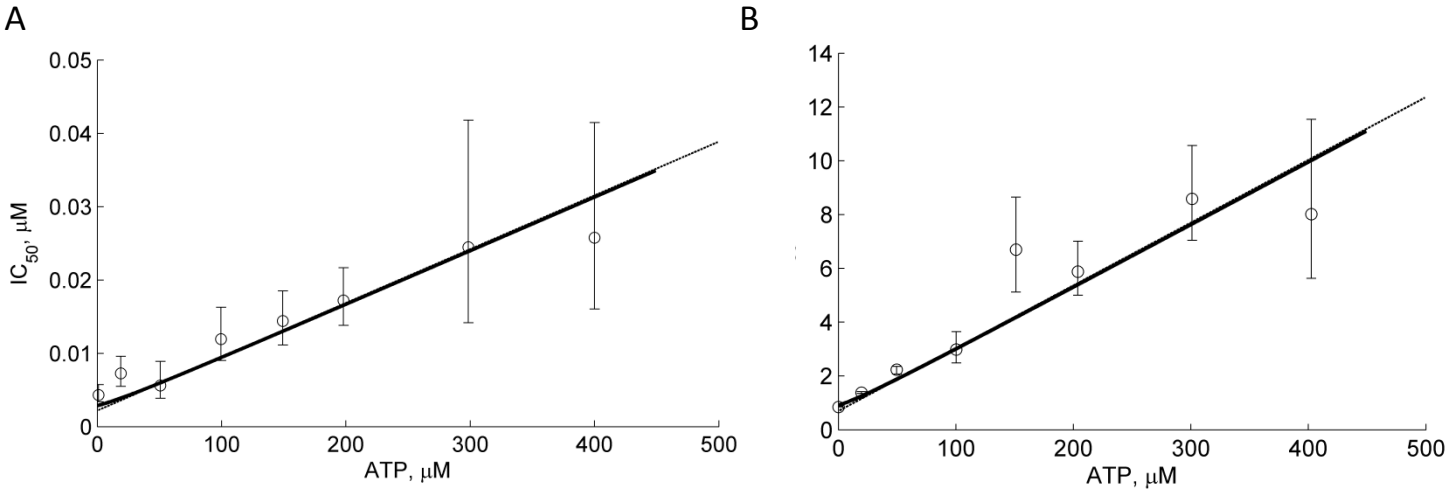
A
B
0.05
0.04
0.03
0.02
0.01
0
IC50, μM
0
100
200
300
400
500
ATP, μM
14
12
10
8
6
4
2
0
ATP, μM

Fig. 8.

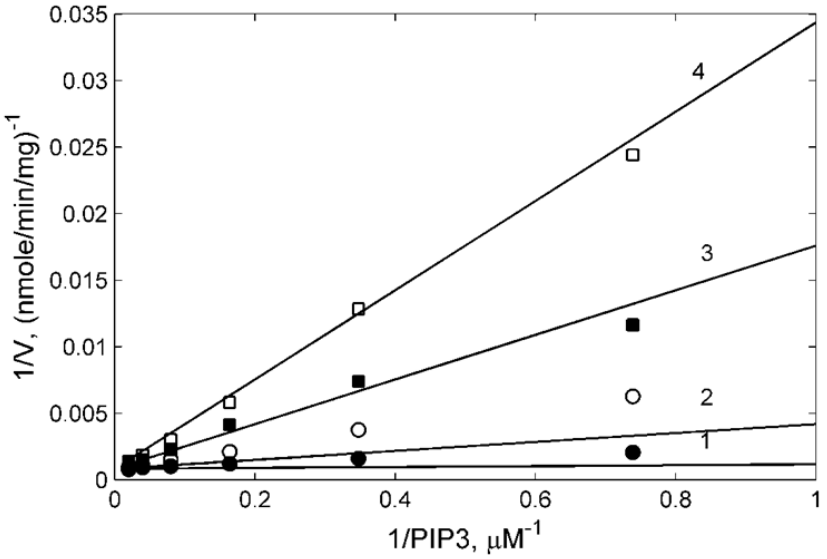
0.035
0.03
0.025
0.02
0.015
0.01
0.005
0
1/V, (nmole/min/mg)-1
4
3
2
1
0
0.2
0.4
0.6
0.8
1
1/PIP3, μM-1

Fig. 9.